

# Block-Diagonal Guided DBSCAN Clustering

Zheng Xing, *Student Member, IEEE*, and Weibing Zhao, *Member, IEEE*

**Abstract**—Cluster analysis plays a crucial role in database mining, and one of the most widely used algorithms in this field is DBSCAN. However, DBSCAN has several limitations, such as difficulty in handling high-dimensional large-scale data, sensitivity to input parameters, and lack of robustness in producing clustering results. This paper introduces an improved version of DBSCAN that leverages the block-diagonal property of the similarity graph to guide the clustering procedure of DBSCAN. The key idea is to construct a graph that measures the similarity between high-dimensional large-scale data points and has the potential to be transformed into a block-diagonal form through an unknown permutation, followed by a cluster-ordering procedure to generate the desired permutation. The clustering structure can be easily determined by identifying the diagonal blocks in the permuted graph. Thus, the main challenge is to construct a graph with a potential block-diagonal form, permute the graph to achieve a block-diagonal structure, and automatically identify diagonal blocks in the permuted graph. To tackle these challenges, we first formulate a block-diagonal constrained self-representation problem to construct a similarity graph of high-dimensional points with a potential block-diagonal form after an unknown permutation. We propose a gradient descent-based method to solve the proposed problem. Additionally, we develop a DBSCAN-based points traversal algorithm that identifies clusters with high densities in the graph and generates an augmented ordering of clusters. The block-diagonal structure of the graph is then achieved through permutation based on the traversal order, providing a flexible foundation for both automatic and interactive cluster analysis. We introduce a split-and-refine algorithm to automatically search for all diagonal blocks in the permuted graph with theoretically optimal guarantees under specific cases. We extensively evaluate our proposed approach on twelve challenging real-world benchmark clustering datasets and demonstrate its superior performance compared to the state-of-the-art clustering method on every dataset.

**Index Terms**—Cluster analysis, DBSCAN, block-diagonal property, self-representation, graph permutation, diagonal block identification.

## 1 INTRODUCTION

LARGER and larger amounts of data are being collected and stored in databases, which increases the need for efficient and effective analysis methods to implicitly utilize the information in the data [1]. One of the primary tasks in data analysis is cluster analysis, which aims to help users understand the natural grouping or structure in a dataset. The unsupervised nature of clustering algorithms makes them widely applicable across diverse domains, including data analysis, computer vision, and image processing [2], [3]. Despite numerous clustering algorithms proposed from various perspectives, it remains challenging to develop an algorithm that can accurately discover clusters from the spatial distribution of data, especially when the number, densities, orientations, and shapes of the underlying clusters are unknown [4].

Traditional clustering algorithms can be categorized into four main types, including partition-based, hierarchical, graph-based, and density-based methods [4]. • The widely used K-means [5] algorithm and its extensions fall under the partition-based category, suitable for finding convex-shaped clusters and relatively easy to implement. However, determining the cluster number  $K$  and initializing the clustering assignment to converge towards a better local optimal

solution are always challenging. • Hierarchical clustering algorithms [6], [7] create a cluster hierarchy by merging clusters based on proximity and interconnectivity, which is effective in discovering clusters with diverse shapes and densities. These methods iteratively merge clusters until the minimum dissimilarity between clusters reaches a certain threshold. However, this method requires the specification of parameters such as the distance metric, linking approach, and number of clusters, which can be challenging to determine accurately. Moreover, once undesired grouping occurs during the merging process, they cannot be corrected in the subsequent clustering steps, leading to inaccurate clustering results. • Graph-based approaches [8] aim to identify dense regions in the graph by maximizing intra-cluster similarity or minimizing inter-cluster similarity. One approach involves identifying the tree structure of the graph, such as the minimum spanning tree [9], which may result in less robust clustering as it prunes the graph to the simplest form, making it susceptible to inaccurate connection caused by noise. Another approach involves solving an optimization problem, such as spectral clustering [10] and its extensions, e.g., [11], which addresses the graph-cut problem through spectral relaxation. However, spectral clustering involves approximation, which can lead to potential performance degradation, and it relies on K-means clustering, which has limitations of its own. • Density-based clustering algorithms have proven successful in discovering clusters of both convex and non-convex shapes. Prominent examples include the widely used Density-Based Spatial Clustering of Applications with Noise (DBSCAN) algorithm [12] and its variants, such as Hierarchical DBSCAN [13] and ST-DBSCAN [14]. Despite the fact that many recently devel-

• Zheng Xing is with Future Network of Intelligence Institute, School of Science and Engineering, The Chinese University of Hong Kong, Shenzhen, China. E-mail: zhengxing@link.cuhk.edu.cn.

• Weibing Zhao is with Guangdong Laboratory of Machine Perception and Intelligent Computing, Shenzhen MSU-BIT University, China. E-mail: weibingzhao@smbu.edu.cn.

Manuscript submitted August 2, 2023; revised January 13, 2024 and April 5, 2024; accepted X X, 2024. (Corresponding author: Weibing Zhao.)

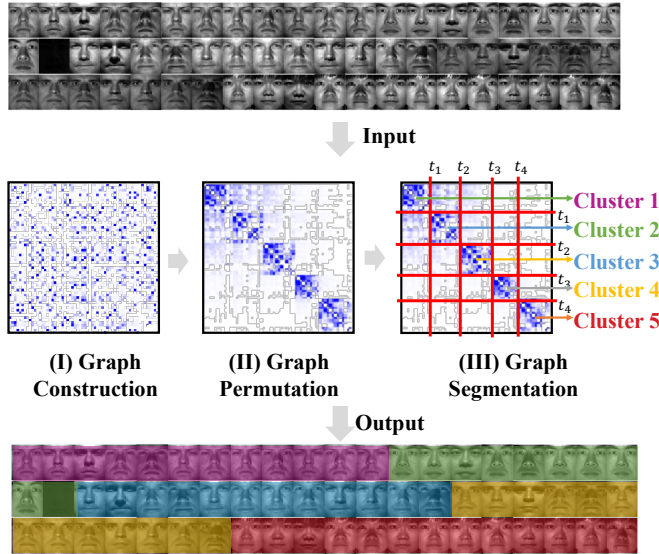


Fig. 1. The framework of the proposed BD-DBSCAN clustering method, including graph construction, permutation, and segmentation. The input is 60 images from Extended Yale-B [15] dataset. The output is the pictorial representation of the cluster assignments for the 60 images. Faces with the same color belong to the same cluster.

oped extensions of DBSCAN have demonstrated relatively good clustering performance, they still suffer from several deficiencies, such as difficulty in handling high-dimensional large-scale data, sensitivity to input parameters, and lack of robustness in producing clustering results.

This paper introduces an improved version of DBSCAN called *Block-Diagonal guided DBSCAN (BD-DBSCAN)*, which involves three stages, as illustrated in Fig. 1. The key idea is to achieve clustering by leveraging the block-diagonal property of the similarity graph. Specifically, to overcome the limitations of DBSCAN in handling high-dimensional large-scale data. We assume that high-dimensional data belonging to the same cluster share the same linear subspace, and thus each of them can be linearly represented by the others. The coefficients of this linear representation can be considered as the similarity between points [16], [17], [18], [19]. Because the similarity within clusters is high and the similarity between clusters is low, the similarity graph has the potential to exhibit a block-diagonal form through an unknown permutation to make clusters in order, which is called the block-diagonal property of the graph. In order to fully utilize and explore the block-diagonal property of the graph, we adopt the following strategies: First, we should guarantee the graph generated by our self-representation learning has the potential to show a block-diagonal form through an unknown permutation of points to make clusters in order. Second, we should search for dense clusters one by one in the graph which can output the desired permutation. Third, we should efficiently identify diagonal blocks in the permuted graph. Thus, we need to address the following three major **challenges**:

- How to construct a similarity graph that has the potential to be transformed into a block-diagonal form after an unknown permutation?
- How to permute a graph into a block-diagonal form?
- How to identify the diagonal blocks in the permuted

graph efficiently?

In this paper, we introduces an improved version of DBSCAN that leverages the block-diagonal property of the similarity graph to guide the clustering procedure of DBSCAN. Specifically, we first present a block-diagonal constrained self-representation problem. The objective is to encourage each point to be represented by points that belong to the same cluster. Additionally, a quadratic regularization term is proposed to constrain the generated similarity matrix to exhibit a block-diagonal form after undergoing an unknown permutation. The graph construction problem is efficiently solved by a proposed gradient descent-based algorithm with guaranteed convergence. Next, inspired by DBSCAN, we introduce a density-based cluster traversal algorithm, which effectively identifies dense clusters in the graph and generates an augmented ordering of points representing the ordered clustering structure. By permuting the graph according to this traversal order, the graph can be transformed into a block-diagonal form. This block-diagonal graph serves as a versatile foundation for both automatic and interactive cluster analysis. It enables graphical representation of clusters, exploration of the intrinsic clustering structure, and provides insights into data distribution and correlation. The clustering structure can be identified by directly counting the number of diagonal blocks, allowing us to explore the intrinsic clustering patterns within each of these blocks. We observe that identifying diagonal blocks in the graph is equivalent to searching for a set of segmentations (such as  $t_1, t_2, \dots, t_4$  in Fig. 1) that can cut the diagonal blocks of the graph ideally. Therefore, we formulate the diagonal block identification problem as a search for a set of segmentation indexes. Our goal is to find segmentation indexes that maximize the sum of the elements in the diagonal blocks, effectively partitioning the graph similarity matrix into an ideal  $K$ -block-diagonal form. To summarize, we make the following **contributions**:

- We present an enhanced version of DBSCAN utilizing a block-diagonal property of the similarity graph which comprises three key stages: graph construction, graph permutation, and graph segmentation. The block-diagonal characteristics is utilized not only to guide the graph construction procedure but also to guide the procedure of identification of the clustering structure. We propose three problems for these three stages and develop efficient algorithms to solve them.
- The proposed clustering method possesses several advantages: (i) it is not sensitive to input parameters, (ii) it can discover clusters with different densities, (iii) it can identify both convex and non-convex shaped clusters, (iv) it allows for visualization of the clustering procedure, (v) it is robust to identify the clustering structure, and (vi) it can handle high-dimensional large-scale datasets with low computational complexity.
- We extensively evaluate our method on real-world benchmark clustering datasets from the literature and compare it with recently developed clustering methods. Our method consistently achieves the highest clustering accuracy, demonstrating the superiority of our proposed approach over state-of-the-art clustering methods.

TABLE 1  
Important notations used throughout the paper

Notation	Description
$K$	The number of clusters
$D$	The dimension of data
$N$	The number of data points
$\mathbf{X} \in \mathbb{R}^{D \times N}$	Data matrix
$\mathbf{x}_i \in \mathbb{R}^D$	Data point
$S_k$	The $k$ -th subspace
$\mathbf{Z} \in \mathbb{R}^{N \times N}$	The self-representation coefficient of $\mathbf{X}$
$z_{i,j}$	The $(i, j)$ -th element of $\mathbf{Z}$
$\mathbf{Y} \in \mathbb{R}^{D \times N}$	The noise matrix
$\tilde{\mathbf{X}}_k \in \mathbb{R}^{D \times N_k}$	Data matrix belonging to the $k$ -th cluster
$\tilde{\mathbf{Z}}^* \in \mathbb{R}^{N \times N}$	The block-diagonal matrix from permuting $\mathbf{Z}$
$\mathbf{\Gamma} \in \mathbb{R}^{N \times N}$	The permuting matrix
$\tilde{\mathbf{Z}}_k^* \in \mathbb{R}^{N_k \times N_k}$	The self-representation coefficient of $\tilde{\mathbf{X}}_k$
$\mathbf{E} \in \mathbb{R}^{N \times N}$	The all-ones matrix
$\mathcal{Z}$	The feasible set of $\mathbf{Z}$
$\mathcal{P}_{\mathcal{Z}}$	The projection operator
$\rho_m$	The spectral step length
$\gamma_m$	The gradient
$\alpha_m$	The step length
$\varepsilon$	The convergence tolerance
$C_{1,1}, C_{1,2}, C_2$	The clusters
$\epsilon, \epsilon_1, \epsilon_2$	The radius of neighborhood
$\delta$	Minimum number of points in neighborhood
$\mathbf{W}$	The similarity matrix
$w_{i,j}$	The $(i, j)$ -th element of $\mathbf{W}$
$c_i$	Similarity between $i$ th sample and its $\delta$ th neighbor
$Q$	The queue
$t_i$	The true partition indexes
$\tau_m$	The estimated partition indexes
$\mathcal{C}_k$	The assignment set of the $k$ -th cluster

The remainder of the paper is structured as follows. In Sec. 2, we introduce the related works of our paper, encompassing DBSCAN clustering and block-diagonal guided clustering methods. In Sec. 3, we introduce our proposed techniques for graph construction, permutation, and segmentation. The experimental results are presented in Sec. 4, and the paper is concluded in Sec. 5. For clarity, the notations adopted throughout the paper are summarized in Tab. 1.

## 2 RELATED WORK

### 2.1 DBSCAN Clustering

Let us give a brief outline of the DBSCAN firstly. Suppose we have an undirected graph  $\mathcal{G} = (\mathcal{V}, \mathbf{W})$ , where  $\mathcal{V}$  is the point set, and the element  $w_{p,q} \geq 0$  in  $\mathbf{W}$  saves the edge weight (similarity) between point  $p$  and point  $q$ . The greater the weight, the closer the distance between two points. DBSCAN starts by pruning the graph to a weighted  $\epsilon$ -Nearest-Neighbor Graph ( $\epsilon$ -NNG), where  $\epsilon$  is the radius of neighborhood. An edge  $w_{p,q}$  between two vertexes  $p, q$  in graph  $\mathcal{G}$  is set to be zero if  $w_{p,q} < \epsilon$ . Denote  $\mathcal{N}_\epsilon(p)$  as the  $\epsilon$ -radius neighborhood of point  $p$ , i.e.,  $\mathcal{N}_\epsilon(p) = \{q \in \mathcal{V} : w_{p,q} \geq \epsilon\}$ . DBSCAN constructs its MST (minimal spanning tree) and then finds the connected components in the MST [20]. These components are the desired clustering.

The detail of DBSCAN [12] to search clusters is shown below. DBSCAN [12] detects high-density spatial regions and expands them to form clusters. It has two hyper-parameters: the radius of neighborhood  $\epsilon$  and the minimum number of points  $\delta$  (also found as *minPts* in the literature).

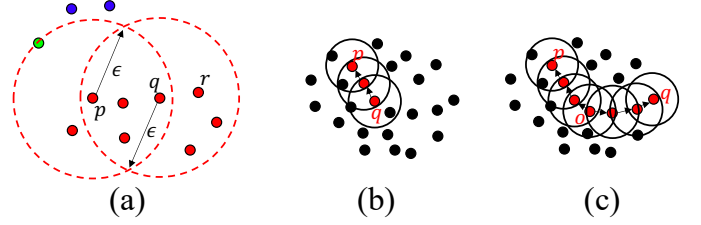


Fig. 2. Key definitions in DBSCAN. (a): the hyper-parameters that control the algorithm are  $\epsilon$  and  $\delta = 3$  in this example. A core point is red, a border point is green dot, and a noise point blue. Point  $q$  is directly  $\epsilon$ -reachable from  $p$  since  $q \in \mathcal{N}_\epsilon(p)$ ; For points  $q$  and  $r$ , it is easy to see that they are both directly  $\epsilon$ -reachable from each other; (b):  $p$  is  $\epsilon$ -reachable from  $q$ ; (c):  $p$  and  $q$  are  $\epsilon$ -connected.

Using these parameters points are classified into three different types in Definition 1 based on density, i.e., core points, border points and noise points.

**Definition 1** (classification of points). *Given  $\epsilon$  and  $\delta$ , DBSCAN classifies points  $\mathcal{V}$  into three types:*

- *core points:*  $\mathcal{V}_{\text{core}} = \{p \in \mathcal{V} : |\mathcal{N}_\epsilon(p)| \geq \delta\}$ .
- *border points:*  $\mathcal{V}_{\text{border}} = \{p \in \mathcal{V} - \mathcal{V}_{\text{core}} : \exists q \in \mathcal{V}_{\text{core}}, \text{ s.t. } p \in \mathcal{N}_\epsilon(q)\}$ .
- *noise points:*  $\mathcal{V}_{\text{noise}} = \mathcal{V} - \mathcal{V}_{\text{core}} - \mathcal{V}_{\text{border}}$ .

DBSCAN uses three pairwise-point relations, which we give below in Definitions 2, 3 and 4.

**Definition 2** (direct  $\epsilon$ -reachable). *A point  $q$  is directly  $\epsilon$ -reachable from a point  $p$  if  $p \in \mathcal{V}_{\text{core}}$ , and  $q \in \mathcal{N}_\epsilon(p)$ , which is denoted by  $p \xrightarrow{\epsilon} q$ .*

**Definition 3** ( $\epsilon$ -reachable). *A point  $q$  is  $\epsilon$ -reachable from a point  $p$  if  $p \in \mathcal{V}_{\text{core}}$  and  $\exists p_1, p_2, \dots, p_n \in \mathcal{V}_{\text{core}}$ , s.t.  $p \xrightarrow{\epsilon} p_1, p_1 \xrightarrow{\epsilon} p_2, \dots, p_n \xrightarrow{\epsilon} q$ , which is denoted by  $p \xrightarrow{\epsilon} q$ .*

**Definition 4** ( $\epsilon$ -connected). *A point  $p$  is  $\epsilon$ -connected with  $q$  if  $\exists o \in \mathcal{V}_{\text{core}}$ , s.t.  $o \xrightarrow{\epsilon} p$  and  $o \xrightarrow{\epsilon} q$ , which is denoted by  $p \xleftrightarrow{\epsilon} q$ .*

Using these definitions, a density-based cluster in DBSCAN given by Definition 5.

**Definition 5** (cluster of DBSCAN). *A DBSCAN cluster  $\mathcal{C}$  is a nonempty subset of points in  $\mathcal{V}$  satisfying that:*

- $\forall p, q \in \mathcal{V}$ : if  $p \in \mathcal{C}$  and  $p \xrightarrow{\epsilon} q$ , then  $q \in \mathcal{C}$ . (Maximality)
- $\forall p, q \in \mathcal{C}$ :  $p \xleftrightarrow{\epsilon} q$ . (Connectivity)

Fig. 2 illustrates the basic concepts of DBSCAN. Fig. 2 (a) illustrates the definitions on a database of 2-dimensional points from a metric space, and the exponential negative distance measure is set to be the edge weight. For core points, the relation of  $\epsilon$ -reachable is equivalent to the relation of  $\epsilon$ -connected, and this relation is an equivalence relation, i.e., it's symmetric, transitive and reflexive. By Definition 5, the DBSCAN clusters restricted to core points are equivalence classes defined by the relation of  $\epsilon$ -reachable. Thus, a core point belongs to a unique cluster. By the connectivity in Definition 5 (ii), a border point could belong to any cluster that contains core point in the  $\epsilon$ -radius neighborhood of border point. A noise point belongs to no cluster. Therefore, from the implementation point of view, DBSCAN is interested in clustering core points. Fig. 2 (b) and (c) illustrate  $\epsilon$ -reachable and  $\epsilon$ -connected in Definition 3 and 4.

The main *shortcomings* of DBSCAN are that [21]:

- Constructing a graph for high-dimensional large-scale data is expensive. Moreover, the distance metrics (e.g., Euclidean, Chebyshev, Cosine, etc) are only exploited to describe local relationships in data space, and have limitation to represent the relationship of high-dimensional data.
- The structure of  $\epsilon$ -NNG becomes increasingly sensitive to the parameter  $\epsilon$  with increasing dimension: small perturbations in  $\epsilon$  can turn a very sparse graph into a very dense one. Additionally,  $\delta$  determines the partition of points into core, border, and noise points, and slight changes in  $\epsilon$  can lead to different  $\epsilon$ -connected results. Moreover, if the density of different clusters is different, and  $\epsilon$  and  $\delta$  are not properly set, DBSCAN may easily mis-classify low-density cluster points as noise, or mis-classify noise as border or core points.
- Finding connected components in  $\epsilon$ -NNG based on connectivity alone is not robust to noisy datasets. There exists a case where all points in  $\epsilon$ -NNG are connected by noise points, resulting in only one cluster according to DBSCAN.

In [22], the author presents a theoretical analysis of the performance and convergence of DBSCAN with increasing  $N$ , demonstrating the effectiveness of DBSCAN in clustering. In [23], the authors propose SNG-DBSCAN, which runs in  $\mathcal{O}(N \log N)$  time to reduce complexity by sub-sampling the edges of the neighborhood graph. In [24], the authors introduce PDBSCAN, which uses a KD-tree to construct a more accurate  $\epsilon$ -NNG. The same group proposes OPTICS, a DBSCAN-like clustering algorithm [20], which achieves similar performance by separating the procedure of DBSCAN into two stages, reducing sensitivity to input parameters. In [25], the authors introduce PARDICLE to construct an approximate  $\epsilon$ -graph by estimating point density and restricting exact neighborhood searches to a small number of points. This approach is designed to use less memory and computation, as FLANN [26] does not support distributed-memory parallelism. The authors in [27] address problems with  $d > 3$  and propose an MPI-based implementation of the algorithm. The work in [28] proposes a KNN-DBSCAN algorithm to symmetrize the k-NNG graph by dropping all single-direction edges and then using exact  $\epsilon$ -searches. The works [29], [30] are specifically designed for 2D/3D datasets and provide guaranteed clustering performance.

Almost all of the studies exclusively concentrate on addressing specific drawbacks of DBSCAN, resulting in only marginal improvements in clustering performance compared to DBSCAN. Numerous experiments have shown that both DBSCAN and its extensions exhibit poor performance when dealing with high-dimensional large-scale datasets.

## 2.2 Block-Diagonal Guided Clustering

Numerous works leverage the block-diagonal properties of the similarity graph to enhance clustering performance by similarity matrix optimization. Subsequently, they depend on spectral clustering to identify the clustering structure, utilizing the spectrum (eigenvalues) of the similarity matrix for dimensionality reduction and applying K-means clustering in fewer dimensions. However, these methods identify the clustering structure without fully utilizing the

block-diagonal property as guidance, potentially leading to unsatisfactory clustering results. For instance, Feng et al. [31] propose a graph Laplacian constraint-based formulation to construct an exactly block-diagonal similarity matrix, making it the first attempt to explicitly pursue such a structure. Wu et al. [32] integrate a block-diagonal prior into the construction of a similarity matrix to improve clustering accuracy on sequential data. Lee et al. [33] introduce the membership representation to detect block-diagonal structures in the output of graph construction. Xie et al. [34] propose an implicit block-diagonal low-rank representation model by incorporating implicit feature representation and block-diagonal prior into the prevalent low-rank representation method. Lu et al. [35] develop a general formulation for constructing similarity graphs and provide a unified theoretical guarantee of the block-diagonal property. Yang et al. [36] propose a joint robust multiple kernel clustering method that encourages the acquisition of an affinity matrix with optimal block-diagonal properties based on a block-diagonal regularizer and the self-expressiveness property. Liu et al. [37] propose a spectral-type clustering scheme that directly pursues the block-diagonal structure of the similarity graph using a special K-block-diagonal constraint. Wang et al. [38] introduce a non-convex regularizer to constrain the affinity matrix and exploit the block-diagonal structure. Qin et al. [39] propose a new semi-supervised clustering approach that flexibly enforces the block-diagonal structure on the similarity matrix while considering sparseness and smoothness simultaneously. Lin et al. [40] propose an adaptive block-diagonal representation approach that explicitly pursues the block-diagonal structure without sacrificing the convexity of the optimization problem. Liu et al. [41] introduce an adaptive low-rank kernel block-diagonal representation graph construction algorithm. They map the original input space into a kernel Hilbert space that is linearly separable and then apply spectral clustering in the feature space. Qin et al. [42] establish an explicit theoretical connection between spectral clustering [43] and graph construction with block-diagonal representation. Xu et al. [44] propose a novel approach called projective block-diagonal representation, which rapidly pursues a representation matrix with block-diagonal structure. Li et al. [45] present an enforced block-diagonal graph learning method for multi-kernel clustering. They pursue a high-quality block-diagonal graph using a well-designed one-part graph learning scheme. Kong et al. [46] introduce block-diagonal regularization to ensure that the obtained representation matrix involves a  $k$ -block-diagonal, where  $k$  denotes the number of clusters. Li et al. [47] propose a method to construct a block-diagonal similarity matrix with ordered partition points based on the  $l_2$ -norm. The block-diagonal research has also been applied to multi-view clustering, as seen in works such as Yin et al. [48], and Liu et al. [49]. Other matrix optimization-based methods include [41], [45], [46], [50], [51], [52], [53].

Recently, neural network-based approaches have attracted more attention. For instance, Xu et al. [54] proposed a novel latent block-diagonal representation model for graph construction on nonlinear structures. Their approach jointly learns an auto-encoder and a similarity matrix with a block-diagonal structure. Liu et al. [49] integrated the block diagonal and diverse representation into the network and



proposed a multi-view subspace clustering network with the block diagonal and diverse representation. Other neural network-based works include [55], [56], [57].

While some methods aim to identify the block-diagonal structure in the similarity matrix for clustering, they fail to incorporate block-diagonal guidance when constructing the similarity graph. Consequently, the block-diagonal structure of the similarity matrix itself remains unclear. This difficulty in identifying the block-diagonal in the similarity graph often leads to unsatisfactory clustering results. For instance, [58] proposed generating block-diagonal forms to provide an intermediate clustering result, facilitating exploration of machine groups and part families before specifying structural criteria. [59] designed the diagonal block model to identify representative block cluster structures from the similarity matrix. [60] rearranged the binary (or 0-1) machine-part matrix into a compact block-diagonal form combining the properties of the minimal spanning tree and cell design analyses. [61] introduced a generative model for clustering, identifying the block-diagonal structure of the similarity matrix to ensure that samples within the same cluster (diagonal block) are similar, while samples from different clusters (off-diagonal block) are less similar. [62] proposed a novel method named multiple kernel k-means clustering with block-diagonal property.

### 3 METHODOLOGY

In this section, we begin by introducing a block-diagonal constrained self-representation problem for constructing the similarity graph (Sec. 3.1). Subsequently, we present an algorithm inspired by DBSCAN to rearrange the graph into a block-diagonal structure (Sec. 3.2). Lastly, we propose an efficient algorithm to identify the diagonal blocks in the permuted graph, ensuring optimality under a specific case (Sec. 3.3).

#### 3.1 Constructing Similarity Graph with Block-Diagonal Constraint

Our algorithm starts by constructing a similarity graph of the input high-dimensional points. The traditional distance measurement methods, such as Euclidean, Chebychev, Cosine, Hamming, and Spearman [63], which use the spatial proximity of the data to measure the distance between points are not applicable to high-dimensional data. It is now widely known that the high dimensional data can be modeled as samples drawn from the union of multiple low-dimensional linear subspaces [16], [17], [18], [19], [64], with each subspace corresponding to a cluster or category. In this section, we are interested in constructing the relationship between data points and a number of subspaces with each cluster corresponding to one of subspaces. Note that, with the assumption that the sampled data have the approximately linear subspace structure. Such data points are not necessarily locally distributed.

**Definition 6.** [Subspace aggregation of high-dimensional data] Given sufficient data  $\mathbf{X} = [\mathbf{x}_1, \mathbf{x}_2, \dots, \mathbf{x}_N] \in \mathbb{R}^{D \times N}$  with a large enough  $D$ . Without loss of generality, assume these data are drawn from  $K$  ( $K$  is known or unknown) linear subspaces  $\mathcal{S}_k \subset \mathbb{R}^D$ ,  $k \in \{1, 2, \dots, K\}$ , of arbitrary dimensions  $d_k \ll D$ . If the

similarity between data is calculated according to the underlying subspaces they are drawn from, the similarity of two points is zero if they are located in different subspace, and larger than zero otherwise.

**1) Optimization Target.** In order to learn the graph for the high-dimensional data, lots of works [16], [17], [18], [19] express that each high-dimensional datum  $\mathbf{x}_i \in \mathcal{S}_k$  as the linear combination of all other data  $\mathbf{x}_i = \sum_{j \neq i} z_{i,j} \mathbf{x}_j$ , and implicitly enforce those coefficients  $z_{i,j}$  to be zero for all  $\mathbf{x}_j \notin \mathcal{S}_k$  under certain assumptions. That is to learn a coefficient matrix  $\mathbf{Z} \in \mathbb{R}^{N \times N}$  such that  $z_{i,j} = 0$  if  $\mathbf{x}_i$  and  $\mathbf{x}_j$  belong to different subspaces.

This paper also expresses each point  $\mathbf{x}_i$  as the linear combination other points. However, we propose a quadratic regularization term on  $\mathbf{Z}$  to enforce the coefficients of vectors  $\mathbf{x}_j \notin \mathcal{S}_k$  to be zero under certain assumptions. Specifically, to take the possible noises into consideration, we express  $\mathbf{X}$  to be  $\mathbf{X} = \mathbf{XZ} + \mathbf{Y}$ , where  $\mathbf{Y}$  is the noise term. We take the Frobenius norm on  $\mathbf{Y}$  as the loss function to penalize misfit. Moreover, we propose  $\|\mathbf{Z}^T \mathbf{Z}\|_1$  to enforce the *block-diagonal* structure of  $\mathbf{Z}$ . The final formulation is given by the following constrained optimization problem:

$$\begin{aligned} & \underset{\mathbf{Z}}{\text{minimize}} \quad \|\mathbf{X} - \mathbf{XZ}\|_F^2 + \lambda \|\mathbf{Z}^T \mathbf{Z}\|_1 \\ & \text{subject to} \quad \mathbf{Z} \geq \mathbf{0}, \text{diag}(\mathbf{Z}) = \mathbf{0} \end{aligned} \quad (1)$$

where  $\|\mathbf{A}\|_F = \sqrt{\sum_i \sum_j a_{i,j}^2}$  is the Frobenius norm of  $\mathbf{A}$ ,  $\|\mathbf{A}\|_1 = \sum_i \sum_j |a_{i,j}|$  is the one norm of  $\mathbf{A}$ , and  $\text{diag}(\mathbf{A})$  is the diagonal vector of matrix  $\mathbf{A}$ . Since  $\mathbf{X} - \mathbf{XZ} = [\mathbf{x}_1 - \sum_j z_{1,j} \mathbf{x}_j, \mathbf{x}_2 - \sum_j z_{2,j} \mathbf{x}_j, \dots, \mathbf{x}_N - \sum_j z_{N,j} \mathbf{x}_j]$ , minimizing  $\|\mathbf{X} - \mathbf{XZ}\|_F^2 = \sum_i \sum_j (x_{i,j} - \sum_j z_{i,j} x_{i,j})^2$  will force  $\mathbf{Z}$  to be sparse, and the element in  $\mathbf{Z}$  measures the similarity between points [16].

**Theorem 1.** Let  $\mathbf{X} \in \mathbb{R}^{D \times N}$  be a matrix whose columns are drawn from a union of  $K$  orthogonal linear subspaces  $\{\mathcal{S}_1, \mathcal{S}_2, \dots, \mathcal{S}_K\}$ . Let  $\mathbf{\Gamma}$  be a permutation matrix such that  $\tilde{\mathbf{X}} = \mathbf{X}\mathbf{\Gamma} = [\tilde{\mathbf{X}}_1, \tilde{\mathbf{X}}_2, \dots, \tilde{\mathbf{X}}_K]$ , where  $\tilde{\mathbf{X}}_k$  is an  $D \times N_k$  matrix whose columns lie in the same subspace  $\mathcal{S}_k$ , and  $N_1 + N_2 + \dots + N_K = N$ . The solution  $\mathbf{Z}^*$  to (1) satisfies the property that  $\tilde{\mathbf{Z}}^* = \mathbf{\Gamma}^{-1} \mathbf{Z}^* \mathbf{\Gamma} = \text{diag}(\tilde{\mathbf{Z}}_1^*, \tilde{\mathbf{Z}}_2^*, \dots, \tilde{\mathbf{Z}}_K^*)$ , which is a  $N$ -by- $N$  block-diagonal matrix with the  $k$ -th diagonal block  $\tilde{\mathbf{Z}}_k^* \in \mathbb{R}^{N_k \times N_k}$ .

*Proof.* See Appendix A.  $\square$

With the constraint of the proposed term  $\|\mathbf{Z}^T \mathbf{Z}\|_1$ , Theorem 1 indicates that the solution to problem (1) after an unknown permutation  $\mathbf{\Gamma}$  exhibits a *block-diagonal* structure under the orthogonal linear subspaces assumption. We can also easily prove that, even without the orthogonal subspace assumption, the solution may still have the *block-diagonal* property when  $\lambda$  is large enough.

Theorem 1 serves as a motivation for proposing BD-DBSCAN in this paper. Specifically, given the solution  $\mathbf{Z}^*$  of problem (1), we can find the corresponding permutation matrix  $\mathbf{\Gamma}$  that permutes  $\mathbf{Z}^*$  to a *block-diagonal* form  $\tilde{\mathbf{Z}}^*$ . Then, the clustering structure of the data can be extracted by identifying the diagonal blocks in  $\tilde{\mathbf{Z}}^*$ . Thus, we propose a graph permutation method in Sec. 3.3 and a graph segmentation method in Sec. 3.2.

**2) Problem Solution.** Problem (1) is a convex quadratic programming problem with box constraints. We consider using the conditional gradient descent method to solve the problem.

Let  $\mathbf{E}$  be an all-one matrix. Because  $\mathbf{Z}$  is element-wise nonnegative, the objective function can be re-expressed as  $g(\mathbf{Z}) = \|\mathbf{X} - \mathbf{X}\mathbf{Z}\|_F^2 + \lambda\|\mathbf{Z}^T\mathbf{Z}\|_1 = \text{tr}[\mathbf{Z}^T\mathbf{X}^T\mathbf{X}\mathbf{Z}] - 2\text{tr}(\mathbf{X}^T\mathbf{X}\mathbf{Z}) + \text{tr}(\mathbf{X}^T\mathbf{X}) + \lambda\text{tr}(\mathbf{Z}^T\mathbf{Z}\mathbf{E})$ , where  $\mathbf{E} \in \mathbb{R}^{N \times N}$  is an all-ones matrix. The gradient of the objective function is then given by

$$\nabla g(\mathbf{Z}) = 2\mathbf{X}^T\mathbf{X}\mathbf{Z} - 2\mathbf{X}^T\mathbf{X} + 2\lambda\mathbf{Z}\mathbf{E}.$$

A straightforward approach to solving the problem is to directly utilize the gradient  $\nabla_{\mathbf{Z}}$  and employ gradient descent to find the solution for  $\mathbf{Z}$ . However, Problem (1) is subject to a non-convex constraint. Hence, we also need to consider the constraint conditions when calculating the gradient. Let  $\mathcal{Z} = \{\mathbf{Z} \in \mathbb{R}^{N \times N} | z_{i,i} = 0, z_{i,j} \geq 0, \forall i, j\}$  be the feasible set. We define the projection operator  $\mathcal{P}_{\mathcal{Z}} : \mathbb{R}^{N \times N} \mapsto \mathcal{Z}$  as:

$$\mathcal{P}_{\mathcal{Z}}(\mathbf{Z}) = \begin{cases} z_{i,j} & \text{if } i \neq j, z_{i,j} \geq 0; \\ 0 & \text{otherwise} \end{cases}$$

It's easy to prove that  $\mathcal{P}_{\mathcal{Z}}(\mathbf{Z}) = \text{argmin}_{\tilde{\mathbf{Z}} \in \mathcal{Z}} \|\mathbf{Z} - \tilde{\mathbf{Z}}\|_F$ . The projection  $\mathcal{P}_{\mathcal{Z}}(\mathbf{Z})$  of  $\mathbf{Z}$  is the set of the solution that satisfies the constraint.

Given an initial  $\mathbf{Z}_0$  by the cosine measurement [6] and a spectral step length  $\rho_0 = 1$ . At the  $m$ th iteration, we first compute the gradient  $\gamma_m = \mathcal{P}_{\mathcal{Z}}(\mathbf{Z}_m - \rho_m \nabla g(\mathbf{Z}_m)) - \mathbf{Z}_m$ . Then, we compute the step length  $\alpha_m$  using line search [65], and update the solution  $\mathbf{Z}_{m+1} = \mathbf{Z}_m + \alpha_m \gamma_m$ . Finally, we update the spectral step length  $\rho_m = \frac{[\text{vec}\{\nabla g(\mathbf{Z}_{m+1}) - \nabla g(\mathbf{Z}_m)\}]^T [\text{vec}\{\nabla g(\mathbf{Z}_{m+1}) - \nabla g(\mathbf{Z}_m)\}]}{[\text{vec}\{\rho_m d_m\}]^T [\text{vec}\{\nabla g(\mathbf{Z}_{m+1}) - \nabla g(\mathbf{Z}_m)\}]}$ .

We can use the following criteria to examine the convergence, e.g.  $\|\mathbf{Z}_{m+1} - \mathbf{Z}_m\|_F^2 < \varepsilon$ , where  $\varepsilon$  is pre-defined convergence tolerance, which should be set small if the data are "clean" and should be relatively large if the data are contaminated with heavy data noises. The convergence can be easily proved according to [65].

In general, the graph will be represented by the matrix  $\mathbf{W} = \frac{|\mathbf{Z}| + |\mathbf{Z}|^T}{2}$ , taking into account the symmetric and positive properties of the graph. Here,  $|\mathbf{Z}|$  denotes the matrix obtained by taking the absolute value of each element of  $\mathbf{Z}$ .

### 3.2 Permuting Graph to be Block-Diagonal via Density-Based Cluster-Ordering

DBSCAN has the ability to identify dense clusters in a given graph, as stated in Sec. 2.1. However, it suffers from several drawbacks. One limitation of DBSCAN is its effectiveness in handling high-dimensional large-scale data, which are addressed in Sec. 3.1. Additionally, it is sensitive to the input parameters, and it lacks robustness in producing clustering results. For example, consider the dataset depicted in Fig. 3 (a). It is not possible to detect the clusters  $C_{1,1}$ ,  $C_{1,2}$ , and  $C_2$  simultaneously using one global density parameter. A global density-based decomposition would consist only of the clusters  $C_1$  and  $C_2$ , or  $C_{1,1}$  and  $C_{1,2}$ . In the second case, the objects from  $C_2$  are considered noise. Moreover, if there are noise points between  $C_{1,1}$ ,  $C_{1,2}$ , and  $C_2$ , DBSCAN may

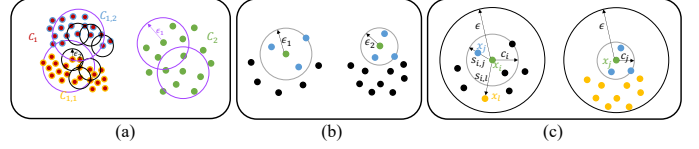


Fig. 3. (a) Clusters wrt. different density parameters; (b) We set  $\delta = 3$ . The cluster with low density requires a larger  $\epsilon$  compared to the cluster with high density, i.e.,  $\epsilon_1 > \epsilon_2$ ; (c) The reachable similarity of points in two clusters with different densities.

output only one cluster containing all points from  $C_2$ ,  $C_{1,1}$  and  $C_{1,2}$  when the parameter values are not appropriately selected for the dataset.

**1) Extended DBSCAN Scheme.** Consider setting  $\epsilon$  for each cluster. As depicted in Fig. 3 (b), we have observed that, for a constant  $\delta$  value, density-based clusters with higher density require a larger value for  $\epsilon$  to ensure that the data within the cluster is identified as core points or border points. On the other hand, density-connected sets with lower density require a smaller value for  $\epsilon$ . This fact is also illustrated in Fig. 3 (a), where  $C_2$  represents density-based clusters with respect to  $\epsilon_1$ , and  $C_{1,1}$ ,  $C_{1,2}$  are density-based clusters with respect to  $\epsilon_2 > \epsilon_1$ . Hence, we introduce the concept of reachable similarity to represent the variation in  $\epsilon$  values among clusters with different densities.

**Definition 7** (reachable similarity). *Let  $i$ th sample be a core point and  $j$ th sample is its direct  $\epsilon$ -reachable, the reachable similarity of  $j$ th sample to the  $i$ th sample is defined as  $s_{i,j} = \min(c_i, w_{i,j})$ , where the  $c_i$  is the similarity between  $i$ th sample and its  $\delta$ -largest-similarity neighbor.*

The value  $c_i$  of the  $i$ th point is defined as the minimum similarity between the  $i$ th sample and its  $\epsilon$ -reachable point. Clearly, points with lower density have smaller values of  $c_i$ , while points with higher density have larger values of  $c_i$ . This way, the density information of different clusters is encapsulated within the  $c_i$  values of different core points. We redefine the similarity measurement when identify the clusters using DBSCAN. Intuitively, the reachable similarity between an object  $j$  and another point  $i$  is the largest similarity such that  $j$  is directly  $\epsilon$ -reachable from  $i$  if  $i$  is a core point. In this case, the reachable similarity cannot be larger than  $c_i$ . The reachable similarity of a point  $j$  depends on the core point with respect to which it is calculated. Fig. 3 (c) illustrates the concepts of the reachable similarity.

The reachable similarity defined above addresses one of the limitation of DBSCAN, that is sensitive to the input parameter. DBSCAN has the chance to identify clusters with different densities under a rough parameter setting of  $\epsilon$  and  $\delta$ , for instance, identify  $C_{1,1}$ ,  $C_{1,2}$ , and  $C_2$  in Fig. 3 (a) simultaneously. Then, we focus on another limitation of DBSCAN, which is the lack of robustness in producing clustering results. Specifically, although DBSCAN can identify clusters with different densities, it may face challenges in effectively identifying and removing noise points between clusters using a rough setting of  $\epsilon$  and  $\delta$ . As a result, two clusters may be identified as one cluster if there exist some noise points between these two clusters, causing these two clusters to be considered  $\epsilon$ -connected by DBSCAN.

To tackle this challenge, we propose to identify clusters

with different densities one by one to generate a permutation order. This way, even if there are a few low-density noise points between clusters, it will not affect our cluster identification procedure. Specifically, the procedure starts by selecting a point in a high-density region (the point with the highest  $c_i$ ) and then iteratively exploring its nearest neighbors with high reachable similarity until there are no unprocessed points  $\epsilon$ -connected to the processed points. Subsequently, we continue iterating through unprocessed points in the same way. This procedure continues until all points have been processed. As a result, points within the same cluster with similar densities will be iterated together. Throughout this procedure, explicit cluster assignment of points is not required. Instead, we preserve the order in which the objects are processed. In contrast to DBSCAN, our approach relies on the measurement of reachable similarity to iterate through clusters one by one. The noise points between two clusters does not influence our cluster-ordering procedure, whereas DBSCAN might identify these two clusters as a single cluster. For instance, as illustrated in Fig. 3 (a), if the points in  $C_{1,1}$  and  $C_{1,2}$  are  $\epsilon$ -connected, we begin with the point exhibiting the highest density and then iterate through the neighboring points located in the same cluster, such as  $C_{1,1}$ . Subsequently, we move on to the nearest cluster  $C_{1,2}$  and iterate through all points within  $C_{1,2}$ . Finally, we proceed to iterate through all points in  $C_2$ . This iterative process allows us to handle different densities effectively and produce more accurate clustering results. Note that, since there is no need to output clustering results, we can set  $\epsilon$  to  $+\infty$ .

**2) Density-Based Cluster Traversal Algorithm.** Based on above analysis, we develop the following traversal procedure. We mark all points as unprocessed. For each unprocessed core point, we perform a cluster order expansion procedure as follows: • Initially, we select one of the unprocessed core points with the highest  $c_i$  (indicating the highest density). This point is marked as processed and added to the order list  $O$ . • Next, an empty priority queue  $Q$  is initialized. We enqueue the indexes of all samples in the  $\delta$ -neighborhood of the selected core point into the queue  $Q$ . The samples are sorted in descending order based on their existing reachable similarity, denoted as  $s_j$ . • While the queue  $Q$  is not empty, we perform the following steps: a. Pop an element  $m$  from the queue  $Q$  (the element with the largest existing reachable similarity). b. Update the existing similarity  $s_j$  for all indexes  $j$  in the  $\delta$ -neighborhood of the element  $m$  if the reachable similarity between index  $j$  and the processing sample  $m$  is larger than the current value of  $s_j$ . c. Push all the indexes of the  $\delta$ -neighborhood of element  $m$  to the queue  $Q$  if the  $m$ th sample is a core point. The elements in the queue  $Q$  are sorted automatically based on their existing reachable similarity. • The order of clusters is recorded in the list  $O$ . Thus, the similarity graph  $\mathbf{W}$  will exhibit a block-diagonal form if it is permuted according to the order list  $O$ .

### 3.3 Identifying Diagonal Blocks in the Graph

In this section, we aim to output the clustering result by identifying the diagonal blocks in the permuted graph. Observed that we only need to search  $K - 1$  partition indexes

$\{t_1, t_2, \dots, t_{K-1}\} \subset \{1, 2, \dots, N\}$  that cut the graph into a *block-diagonal* form with  $K$  blocks. The partition indexes are ordered and unique such that at least one sample is present in each cluster, and  $t_{k-1} < t_k$  for all  $k \in 1, 2, \dots, K$ . The dummy indexes  $t_0 := 0$  and  $t_K := N$  are implicitly available.

**1) Optimization Target.** To obtain the partition index  $\{t_k\}_{k=1}^{K-1}$ , we aim to maximize the sum of similarities within the block diagonals. Specifically, denote the segmentation variable as  $\{\tau_k\}$ . The  $k$ th diagonal block corresponds to the data points indexed by  $C_k = \{\tau_{k-1} + 1, \dots, \tau_k\}$ . The sum of weights in the  $k$ -th diagonal block is represented as  $\sum_{i,j \in C_k} w_{i,j}$ . Intuitively, we might attempt to maximize  $\sum_{k=1}^K \sum_{i,j \in C_k} w_{i,j}$  with respect to the segmentation variable  $\{\tau_k\}$ . However, this approach may inadvertently favor neglecting small clusters. To address this, we introduce a normalization term  $\sum_{i \in C_k} \sum_{j=1}^N w_{i,j}$  into the objective function to balance the size of clusters. Mathematically, the problem is formulated as

$$\begin{aligned} & \text{maximize}_{\{\tau_k\}_{k=1}^{K-1}} \sum_{k=1}^K \frac{\sum_{i,j \in C_k} w_{i,j}}{\sum_{i \in C_k} \sum_{j=1}^N w_{i,j}} \\ & \text{subject to } 0 < \tau_1 < \tau_2 < \dots < \tau_{K-1} < N \end{aligned} \quad (2)$$

Problem (2) is equivalent to minimizing  $\sum_{k=1}^K \text{cut}(C_k, \bar{C}_k) / \text{vol}(C_k)$ , where  $\text{cut}(C_k, \bar{C}_k) = \sum_{i \in C_k} \sum_{j \in \{1, 2, \dots, N\}, j \notin C_k} w_{i,j}$ ,  $\text{vol}(C_k) = \sum_{i \in C_k} \sum_{j \in \{1, 2, \dots, N\}} w_{i,j}$ , which is the traditional Ncut [66] problem. Although the Ncut problem has been studied for many years, its NP-hard nature means that only approximate solutions can be obtained through methods like spectral clustering. This paper introduces a method that, under the condition that  $\mathbf{W}$  is block-diagonal, can achieve the optimal solution to the Ncut problem under specific conditions.

Define

$$f_k(\tau_k; \tau_{-k}) \triangleq \frac{\sum_{i,j \in C_k} w_{i,j}}{\sum_{i=\tau_{k-1}+1}^{\tau_k} \sum_{j=1}^N w_{i,j}} + \frac{\sum_{i,j \in C_{k+1}} w_{i,j}}{\sum_{i=\tau_k+1}^{\tau_{k+1}} \sum_{j=1}^N w_{i,j}}$$

for  $k = 1, 2, \dots, K - 1$ , where  $\tau_{-k} \triangleq (\tau_{k-1}, \tau_{k+1})$ . In addition, define

$$\begin{aligned} f_0(\tau_0) &= \frac{\sum_{i,j \in \{1, 2, \dots, \tau_1\}} w_{i,j}}{\sum_{i=1}^{\tau_1} \sum_{j=1}^N w_{i,j}} \\ f_K(\tau_K) &= \frac{\sum_{i,j \in \{\tau_{K-1}+1, \tau_{K-1}+2, \dots, N\}} w_{i,j}}{\sum_{i=\tau_{K-1}+1}^N \sum_{j=1}^N w_{i,j}} \end{aligned}$$

for mathematical convenience. The problem (2) is equivalent to

$$\begin{aligned} & \text{maximize}_{\{\tau_k\}_{k=1}^{K-1}} \frac{1}{2} \sum_{k=0}^K f_k(\tau_k; \tau_{-k}) \\ & \text{subject to } 0 < \tau_1 < \tau_2 < \dots < \tau_{K-1} < N \end{aligned}$$

In the remaining part of the paper, we may omit the argument  $\tau_{-k}$  and write  $f_k(\tau_k)$  for simplicity, as long as it is clear from the context.

#### 2) The Property of the $f_k(\tau_k)$ in a Special Case.

Consider a special case for  $\mathbf{W}$ . The data points follow the subspace aggregation in Definition 6, and the cluster has been ordered correctly. The inter-cluster similarity of

the  $k$ th cluster can be assumed to be  $w_{i,j} = \mu_k$ , where  $i, j \in \{t_{k-1} + 1, t_{k-1} + 2, \dots, t_k\}$ ,  $k \in 1, 2, \dots, K$ , and the intra-cluster similarity is zero. We observe the following properties for  $f_k(\tau_k)$ .

**Proposition 1** (Unimodality). *Suppose that, for some  $k$ ,  $\tau_{k-1}, \tau_{k+1} \in \{t_0, t_1, \dots, t_K\}$ , there exists only one index  $t_j$ ,  $j \in \{1, 2, \dots, K-1\}$ , within the interval  $(\tau_{k-1}, \tau_{k+1})$ . Then,  $f_k(\tau) - f_k(\tau - 1) > 0$  for  $\tau_{k-1} < \tau < t_j$ , and  $f_k(\tau) - f_k(\tau - 1) < 0$  for  $t_j < \tau < \tau_{k+1}$ . In addition,  $t_j$  minimizes  $f_k(\tau)$  in  $(\tau_{k-1}, \tau_{k+1})$ .*

*Proof.* See Appendix B.  $\square$

This result implies that, once the condition is satisfied, there exists a unique local minima  $t_j$  of  $f_k(\tau)$  over  $(\tau_{k-1}, \tau_{k+1})$ .

**Proposition 2** (Flatness). *Suppose that, for some  $k$ ,  $\tau_{k-1}, \tau_{k+1} \in \{t_0, t_1, \dots, t_K\}$ , there is no index  $t_j \in \{t_1, t_2, \dots, t_{K-1}\}$  in the interval  $(\tau_{k-1}, \tau_{k+1})$ . Then,  $f_k(\tau) - f_k(\tau - 1)$  is constant for  $\tau \in (\tau_{k-1}, \tau_{k+1})$ .*

*Proof.* See Appendix C.  $\square$

It follows that, when the interval  $(\tau_{k-1}, \tau_{k+1})$  does not contain  $t_j$ , the function  $f_k(\tau)$  appears as a flat function for  $\tau \in (\tau_{k-1}, \tau_{k+1})$ .

**Proposition 3** (Monotonicity). *Suppose that, for some  $k$ ,  $\tau_{k-1}, \tau_{k+1} \in \{t_1, t_2, \dots, t_{K-1}\}$ , there are multiple partition indexes  $t_j, t_{j+1}, \dots, t_{j+J} \in \{t_0, t_1, \dots, t_K\}$  within the interval  $(\tau_{k-1}, \tau_{k+1})$ . Then,  $f(\tau) - f(\tau - 1) > 0$  for  $\tau \in [\tau_{k-1}, t_j]$ , and  $f(\tau) - f(\tau - 1) < 0$  for  $\tau \in [t_{j+J}, \tau_{k+1}]$ . Moreover, for any interval  $(t_k, t_{k+1})$ ,  $k \in \{j, j+1, \dots, j+J-1\}$ , there exists a constant  $\hat{\tau}$ , such that*

1) If  $\hat{\tau} \in (t_k, t_{k+1})$ , then  $f(\tau) - f(\tau - 1) > 0$  for  $\tau \in [t_k, \hat{\tau}]$  and  $f(\tau) - f(\tau - 1) < 0$  for  $\tau \in [\hat{\tau}, t_{k+1}]$ ;

2) If  $\hat{\tau} \in [t_{k+1}, N)$ , then  $f(\tau) - f(\tau - 1) > 0$  for  $\tau \in [t_k, t_{k+1}]$ ;

3) If  $\hat{\tau} \in (0, t_k]$ , then  $f(\tau) - f(\tau - 1) < 0$  for  $\tau \in [t_k, t_{k+1}]$ .

*Proof.* See Appendix D.  $\square$

**3) Split-and-Refine Algorithm.** We develop a method for solving problem (2) with an optimal guarantee under the special case of  $\mathbf{W}$ . Specifically, we alternate between adding a new segmentation to the current set of segmentations and then refining the positions of all segmentations until stationarity, i.e., no change of any segmentation improves the objective function value.

In the  $m$ th iteration,  $m = 1, 2, 3, \dots$ , suppose there are  $m$  intervals  $(\tau_{k-1}, \tau_k)$ ,  $k \in \{1, 2, \dots, m\}$  with  $\tau_m = N$ . The  $k$ th interval  $(\tau_{k-1}, \tau_k)$  among  $m$  intervals is selected and split it into two, resulting in a new set of  $m + 1$  intervals. The corresponding  $m$  segmentation indexes are denoted as a  $m$ -tuple  $\boldsymbol{\tau}^{(m,k)} = (\tau_1^{(m,k)}, \tau_2^{(m,k)}, \dots, \tau_m^{(m,k)})$ . Then, we maximize  $f_k(\tau; \boldsymbol{\tau}_{-k}^{(m,k)})$  subject to  $\tau \in (\tau_{k-1}, \tau_{k+1})$ , and denote the minimal value as  $f_*^{(m,k)}$ . In addition, denote the benefit of splitting as

$$\Delta f_*^{(m,k)} = f_*^{(m,k)} - f_k(\tau_{k-1}^{(m,k)}; \boldsymbol{\tau}_{-k}^{(m,k)}) \quad (3)$$

where  $f_k(\tau_{k-1}^{(m,k)}; \boldsymbol{\tau}_{-k}^{(m,k)})$  equals to the objective function value of no splitting.

**Algorithm 1:** The split-and-refine algorithm for searching diagonal blocks.

---

1 **Input:** an ordered graph  $\mathbf{W}$ , and the max number of clusters  $K_{\max}$

2 **Output:** the segmentation  $\boldsymbol{\tau}^{(m)}$ , and the cluster number  $K$ .

3 Initialize  $\boldsymbol{\tau}^{(1)} = \{\}$

4 **for**  $m = 1 : K_{\max} - 1$  **do**

5     **for**  $k = 0 : (m - 1)$  **Parallelly do**

6         a) **Split** the  $k$ th interval into two subsets to form the new segmentation indexes  $\boldsymbol{\tau}^{(m,k)}$ ;

7         b) Compute  $f_*^{(m,k)} = \max\{f_k(\tau; \boldsymbol{\tau}_{-k}^{(m,k)}) : \tau_{k-1}^{(m,k)} < \tau < \tau_{k+1}^{(m,k)}\}$ , and denote the maximizer as  $\tau_k^*$ ; denote  $\hat{\boldsymbol{\tau}}^{(m,k)} = (\tau_1^{(m,k)}, \dots, \tau_{k-1}^{(m,k)}, \tau_k^*, \tau_{k+1}^{(m,k)}, \dots, \tau_m^{(m,k)})$ ;

8         c) Compute the cost reduction  $\Delta f_*^{(m,k)}$  as in (3);

9     Pick  $k^* \triangleq \arg \max_k \Delta f_*^{(m,k)}$ , and assign the segmentation as  $\boldsymbol{\tau}^{(m+1)} = \hat{\boldsymbol{\tau}}^{(m,k^*)}$ .

10 **repeat**

11     **for**  $k = 1 : m$  **do**

12          $\tau_k^* = \arg \max_{\tau_k} f_k(\tau_k)$

13         **if**  $\tau_k^{(m+1)} \neq \tau_k^*$  **then**

14             **Refine**  $\tau_k^{(m+1)} = \tau_k^*$ .

15     **until**  $\{\tau_k^{(m+1)}\}_{k=1}^m$  can not be changed;

16     Save objective function value as  $g(m)$  with the segmentation  $\boldsymbol{\tau}^{(m+1)}$ .

17 **for**  $m = 2, 3, \dots, K_{\max}$  **do**

18     Calculate

19      $g''_m = (g(m) - g(m-1)) - (g(m+1) - g(m))$ .

20  $K = \arg \max_{K \in \{2, 3, \dots, K_{\max} - 1\}} g''_m$

---

As a result,  $\Delta f_*^{(m,k)}$  corresponds to the benefit increase of an optimal split of the  $k$ th interval among  $m$  intervals. Then, by evaluating the benefit increase for all  $m$  possible combinations of the split, one can find the best segmentation variable  $\boldsymbol{\tau}^{(m+1)}$  that yields the most benefit. The overall procedure is summarized in Alg. 1.

The proposed splitting procedure run in a way of searching the segmentation one by one. However, we can not guarantee the final segmentation set is stationary. Thus, we develop a refining procedure after generating a new segmentation. Specifically, after each one segmentation inserting, we perform a refining stage. One can loop over the current segmentation and refine each segmentation alone to maximize the objective. In this step the objective can either increase or stay the same, and we repeat until the current choice of segmentations can not be changed. Moreover, there is no need to call more than once if the segmentations have not changed.

In practice, the number of clusters is often unknown. Therefore, we consider the case that the number of clusters is unknown and set the max cluster number is  $K_{\max}$ . One can insert the segmentation one by one in a serial way until the segmentation number is  $K_{\max}$ . Lines 6 and 7 in



Alg. 1 can be run in parallel over the  $m$  segments. We can also parallelize refining  $m - 1$  segmentations by alternately refining the even and odd segmentations (each of which can be parallelized) until stationarity. Finally, we propose a method to identify the value of cluster number. We save the maximum objective value of problem (2) as  $g(m)$  for cluster numbers  $m = 1, 2, \dots, K^{\max} - 1$ . We assume that the maximum objective value of problem (2) increases as  $K$  increases. We use the second derivative of  $g(m)$  to identify the *inflection point* of the curve  $g(m)$ , which is calculated by  $g_m'' = (g(m) - g(m - 1)) - (g(m + 1) - g(m))$ . The cluster number is determined as  $K = \operatorname{argmax}_{K \in 2, 3, \dots, K^{\max} - 1} g_m''$ .

**Lemma 1** (Cost Reduction). *Consider two distinct intervals  $(\tau_{k-1}^{(m,k)}, \tau_{k+1}^{(m,k)})$  and  $(\tau_{k'-1}^{(m,k')}, \tau_{k'+1}^{(m,k')})$  constructed from the  $m$ th iteration of Step 1) in Alg. 1, where  $\tau_{k-1}^{(m,k)}, \tau_{k+1}^{(m,k)}, \tau_{k'-1}^{(m,k')}, \tau_{k'+1}^{(m,k')} \in t_0, t_1, \dots, t_K$ . Suppose that there exists at least one index  $t_j \in \{t_1, t_2, \dots, t_{K-1}\}$  in  $(\tau_{k-1}^{(m,k)}, \tau_{k+1}^{(m,k)})$ , and no such  $t_j$  in  $(\tau_{k'-1}^{(m,k')}, \tau_{k'+1}^{(m,k')})$ . Then,  $\Delta f_*^{(m,k)} > \Delta f_*^{(m,k')}$ .*

*Proof.* See Appendix E.  $\square$

Lemma 1 can be intuitively understood from Propositions 1 and 2, which suggest that  $f_k(\tau; \tau_{-k}^{(m,k)})$  is unimodal in  $(\tau_{k-1}^{(m,k)}, \tau_{k+1}^{(m,k)})$ , but  $f_{k'}(\tau; \tau_{-k'}^{(m,k')})$  is flat in  $(\tau_{k'-1}^{(m,k')}, \tau_{k'+1}^{(m,k')})$ , and hence, the former one has a larger potential to increase the total benefit  $\sum_{k=0}^m f_k(\tau_k; \tau_{-k})$ .

**Theorem 2** (Optimality). *Alg. 1 will output  $\tau^* = (\tau_1^*, \tau_2^*, \dots, \tau_{K-1}^*)$ , with  $\tau_k^* = t_k, k = 1, 2, \dots, K - 1$ .*

*Proof.* See Appendix F.  $\square$

Theorem 2 provides the optimality guarantee of our Alg. 1 under a special case of W.

## 4 EXPERIMENTAL RESULTS AND ANALYSIS

In this section, we first introduce the datasets used in our experiments (Sec. 4.1), and provide the details of the experimental setup (Sec. 4.2). Then we show the comparison results with several state-of-the-art methods (Sec. 4.3), develop the parameter sensitivity analysis (Sec. 4.4) and conduct the ablation study (Sec. 4.5).

### 4.1 Datasets

To provide a comprehensive evaluation of our proposed model, we perform experiments on eight high-dimensional synthetic datasets with different noise level, and twelve high-dimensional real benchmark clustering datasets.

#### 4.1.1 Synthetic Dataset

The synthetic data samples are generated using the scheme in [68]. Six  $192 \times 168$  images depicting the  $k$ th person in the Extended Yale-B [15] dataset are randomly selected and form a subspace basis matrix  $\mathbf{U}_k = [\mathbf{u}_{k,1}, \mathbf{u}_{k,2}, \dots, \mathbf{u}_{k,6}] \in \mathbb{R}^{32256 \times 6}$ . Then, these images are combined into synthetic samples by using random weights  $\mathbf{w}_{k,i} \in \mathbb{R}^6$  (uniform distribution in  $[0, 1]$ ) such that  $\mathbf{x}_{k,i} = \mathbf{U}_k \mathbf{w}_{k,i}$ . Repeating 100 times, we obtain a set of samples  $\mathbf{X}_k = [\mathbf{x}_{k,1}, \mathbf{x}_{k,2}, \dots, \mathbf{x}_{k,100}]$  from the subspace  $\operatorname{span}(\mathbf{U}_k)$ . Repeating this process for

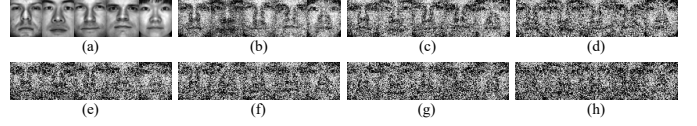


Fig. 4. Examples in the synthetic dataset with different Gaussian noise variance (a) 0, (b) 0.03, (c) 0.06, (d) 0.09, (e) 0.12, (f) 0.15, (g) 0.18, (h) 0.21.

$\mathbf{X}_k$  with  $\mathbf{U}_k$  depicting different persons for five times, i.e.,  $k = 1, 2, \dots, 5$ , we finally get our artificial data  $\mathbf{X} = [\mathbf{X}_1, \mathbf{X}_2, \dots, \mathbf{X}_5] \in \mathbb{R}^{32256 \times 500}$ , which is anticipated to be clustered into five subspaces. To further test the robustness of the proposed methods, we generate another seven datasets by adding Gaussian noise with zero mean and different variances  $\sigma^2 = 0.03, 0.06, 0.09, 0.12, 0.15, 0.18, 0.21$  to the samples  $\mathbf{x}_{k,i}$ , which has been min-max normalized to the interval  $[0, 1]$ . Subsequently, clustering experiments are conducted on these eight datasets. As shown in Fig. 4, as the noise added to the data increases, the distinctiveness between different classes decreases, making clustering more challenging.

#### 4.1.2 Real Dataset

We perform experiments on twelve popular benchmark datasets, including images, texts, and speeches. The number of patterns, the number of clusters, and dimensions of patterns are listed in Tab. 3. The image datasets includes MNIST [69], CIFAR-10 [70], COIL-20 [71], STL-10 [72] and ILSVRC2012-1K [73]. We randomly choose 10 subjects from the ILSVRC2012-1K dataset [73] and resize these images to  $96 \times 96 \times 3$  to construct the ImageNet-10 dataset for our experiments. To compare the clustering methods on more complex dataset, we also randomly select 15 kinds of dog images from ILSVRC2012-1K to establish the fine-grained ImageNet-Dog dataset. The text datasets includes 20NEWS [74], REU-TERS [75], and REUTERS-10k [75] (which is a subset of 10000 texts sampled from REUTERS following [76]). Three speech datasets, i.e., AudioSe t-20, AudioSet-Music, and AudioSet-Human, are randomly chosen from AudioSet [77] for comparison in our experiments. In these datasets, AudioSet-Music and AudioSet-Human are two fine-grained datasets sampled from the coarse classes "Music" and "Human sounds" in AudioSet [77], respectively. Specifically, the term frequency-inverse document frequency features<sup>1</sup> (TF-IDF) and the Mel-frequency cepstral coefficients<sup>2</sup> are employed to recode texts and speeches, respectively.

## 4.2 Experimental Setup

### 4.2.1 Comparisons

We compared our approach to several traditional clustering methods, including: • K-means [5], SpecC [10], and DB-SCAN [12]. We also compared our approach to recently developed clustering methods, including: • Density-based clustering method: FLM [9]. FLM introduces a clustering method using local density peaks-based minimum spanning trees, capable of detecting arbitrarily shaped clusters and

1. <https://scikit-learn.org/stable>

2. <https://librosa.github.io/librosa/feature.html>

TABLE 2  
Clustering performance on synthetic datasets. The first two are marked by **bold** and underline separately.

Variance Metric	0			0.03			0.06			0.09		
	ACC	NMI	ARI	ACC	NMI	ARI	ACC	NMI	ARI	ACC	NMI	ARI
K-means [5]	0.7798	0.8695	0.7440	0.7700	0.8422	0.7396	0.7620	0.8568	0.7378	0.7440	0.8115	0.6959
SpecC [10]	0.8000	0.9057	0.7812	0.7940	0.8776	0.7440	0.7840	0.8615	0.7222	0.7646	0.8215	0.7065
DBSCAN [12]	0.6113	0.7267	0.6129	0.6105	0.6393	0.6089	0.6045	0.6002	0.6075	0.6038	0.5491	0.5816
FLM [9]	0.8666	0.8726	0.7224	0.8011	0.8568	0.6603	0.7854	0.8357	0.8396	0.7993	0.8464	0.7865
AGC [67]	0.8771	0.8986	0.7816	0.8582	0.8195	0.8715	0.8552	0.8948	0.8434	0.8562	0.8393	0.7954
BDF [39]	0.9619	<u>0.9627</u>	0.9150	0.9151	0.8866	0.8752	0.8813	0.8606	0.8454	<u>0.8785</u>	0.8431	0.8691
Ours	<b>1.0000</b>	<b>1.0000</b>	<b>1.0000</b>	<b>1.0000</b>	<b>1.0000</b>	<b>1.0000</b>	<b>0.9900</b>	<b>0.9809</b>	<b>0.9754</b>	<b>0.9620</b>	<b>0.9310</b>	<b>0.9105</b>

Variance Metric	0.12			0.15			0.18			0.21		
	ACC	NMI	ARI	ACC	NMI	ARI	ACC	NMI	ARI	ACC	NMI	ARI
K-means [5]	0.7340	0.8498	0.7179	0.7220	0.7265	0.7102	0.7180	0.7014	0.6867	0.6800	0.6585	0.6045
SpecC [10]	0.7400	0.8582	0.7146	0.7380	0.7529	0.7526	0.7267	0.7433	0.6927	0.7008	0.6676	0.6232
DBSCAN [12]	0.5813	0.5317	0.5149	0.5635	0.5313	0.4699	0.5444	0.5014	0.4475	0.5034	0.4492	0.3617
FLM [9]	0.8461	0.8617	0.7211	0.7910	0.7766	0.7208	0.7259	0.7268	0.5694	0.6598	0.6868	0.5862
AGC [67]	0.8565	0.8284	0.7846	0.7553	0.7675	0.7615	0.7552	0.7447	0.6854	0.7454	0.7196	0.6642
BDF [39]	<u>0.8659</u>	0.8038	0.7468	0.7832	0.7744	0.7556	0.7717	0.7608	<u>0.7056</u>	0.6987	<u>0.7406</u>	0.6320
Ours	<b>0.9540</b>	<b>0.9205</b>	<b>0.8897</b>	<b>0.9120</b>	<b>0.8862</b>	<b>0.8626</b>	<b>0.9000</b>	<b>0.8737</b>	<b>0.8584</b>	<b>0.8880</b>	<b>0.8517</b>	<b>0.8345</b>

TABLE 3  
The property of the high-dimensional benchmark dataset.

Dataset	Numbers	Clusters	Dimensions
MNIST [69]	70000	10	784
CIFAR-10 [70]	60000	10	3072
COIL-20 [71]	1440	20	1024
STL-10 [72]	13000	10	27648
ImageNet-10 [73]	13000	10	27648
ImageNet-Dog [73]	19500	15	27648
20NEWS [74]	18846	20	10000
REUTERS-10k [75]	10000	4	2000
REUTERS [75]	685071	4	2000
AudioSet-20 [77]	30000	20	1920
AudioSet-Music [77]	22500	15	1920
AudioSet-Human [77]	22500	15	1920

being less sensitive to noise and parameters. • Graph-based clustering approach: AGC [67]. AGC proposes a sampling operator for the graph auto-encoder network to protect against noisy clustering assignments and trigger a correction mechanism for feature drift by transforming the graph into a clustering-oriented structure. • Block-diagonal guided clustering method: BDF [39]. BDF presents a semi-supervised approach enforcing block-diagonal structure on the similarity matrix while considering sparseness and smoothness. CSC introduces a graph construction method explicitly pursuing the block diagonal structure through a specially designed convex regularizer that fuses both columns and rows of the coefficient matrix.

#### 4.2.2 Evaluation Metrics and Parameter Settings

We employ three evaluation criteria to assess the clustering performance, namely accuracy (ACC), normalized mutual information (NMI), and refined rand index (ARI). These metrics measure the consistency between the learned labels and the true labels. A higher value for each metric indicates better clustering performance. We set  $\lambda \in [0.1, 2.4]$ , and  $\delta \in [10, 20]$  for our method. For the compared methods, we assign their parameters based on the recommended settings specified in their respective original papers.

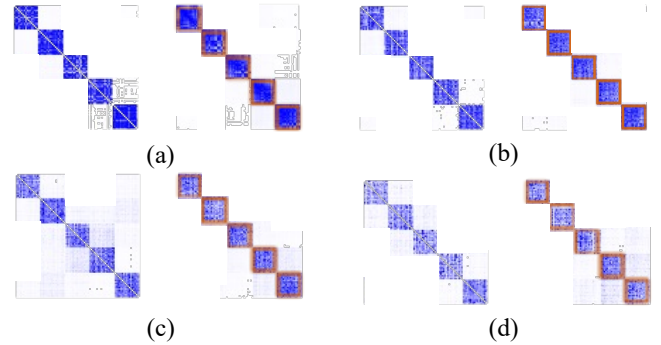


Fig. 5. Visualization on synthetic datasets with different Gaussian noise variance (a) 0, (b) 0.03, (c) 0.06, (d) 0.09. The left figure in (a) shows the result given by our graph construction method, and the right figure in (a) shows our graph permutation result, as well as our block-diagonal identification result (red box).

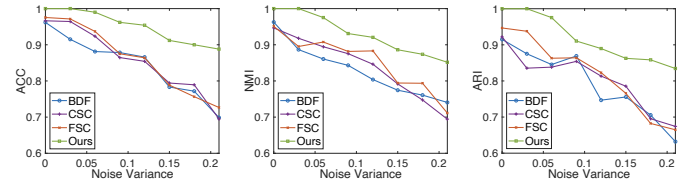


Fig. 6. Clustering performance in presence of different noise variances on the synthetic dataset.

### 4.3 Performance Comparison

#### 4.3.1 Performance on Synthetic Datasets

Tab. 2 presents the performance of our method and the compared methods on the eight synthetic datasets. We have the following observation. • Our BD-DBSCAN method achieves the best performance on all the three evaluation metrics on each dataset. The ACC improvement of our method compared to the second best baseline are 2.46%, 2.86%, 5.31%, 8.35%, 8.81%, 11.78%, 11.06%, and 16.14% respectively, providing compelling evidence of its effectiveness in clustering tasks. Fig. 5 shows the visual results of our method. As depicted in Fig. 5, our DBGO effectively converts the graph into a block-diagonal form and effectively identifies the optimal diagonal block. • Additionally, our method exhibits even more prominent performance on

TABLE 4

The clustering performance of the compared methods on the experimental datasets. The first two are marked by **bold** and underline separately.

Dataset Metric	MNIST [69]			CIFAR-10 [70]			COIL-20 [71]			STL-10 [72]		
	ACC	NMI	ARI	ACC	NMI	ARI	ACC	NMI	ARI	ACC	NMI	ARI
K-means [5]	0.5723	0.4997	0.3652	0.2289	0.0871	0.0487	0.5296	0.4833	0.4283	0.1920	0.1245	0.0608
SpecC [10]	0.6958	0.6626	0.5214	0.2467	0.1028	0.0853	0.6364	0.5941	0.5215	0.1588	0.0978	0.0479
DBSCAN [12]	0.5124	0.4252	0.3169	0.1134	0.0333	0.0388	0.4643	0.4064	0.4478	0.1030	0.0896	0.0310
FLM [9]	0.7430	0.6716	0.6414	0.2401	0.1168	0.0607	0.8852	0.8355	0.7445	0.1590	0.1760	0.0861
AGC [67]	0.8956	0.7884	0.7746	0.2584	0.1616	0.1314	0.8558	0.7941	0.7473	0.2462	0.1399	0.0654
BDF [39]	0.8476	0.7538	0.7350	0.3157	<u>0.2546</u>	0.1758	0.8519	0.8203	0.7423	<u>0.2914</u>	<u>0.2104</u>	0.1398
Ours	<b>0.9852</b>	<b>0.9611</b>	<b>0.9534</b>	<b>0.4828</b>	<b>0.4419</b>	<b>0.3399</b>	<b>0.9962</b>	<b>0.9854</b>	<b>0.9703</b>	<b>0.4819</b>	<b>0.4043</b>	<b>0.2894</b>

Dataset Metric	ImageNet-10 [73]			ImageNet-Dog [73]			20NEWS [74]			REUTERS-10k [75]		
	ACC	NMI	ARI	ACC	NMI	ARI	ACC	NMI	ARI	ACC	NMI	ARI
K-means [5]	0.2409	0.1186	0.0571	0.1054	0.0548	0.0204	0.2328	0.2154	0.0826	0.5242	0.3124	0.2505
SpecC [10]	0.2740	0.1511	0.0757	0.1111	0.0383	0.0133	0.2486	0.2147	0.0934	0.4384	0.3066	0.2301
DBSCAN [12]	0.2171	0.0894	0.0318	0.0756	0.0339	0.0129	0.1905	0.1434	0.0433	0.3676	0.2234	0.1828
FLM [9]	0.2809	0.1819	0.2031	0.1949	0.1216	0.0788	0.5832	0.5286	0.4683	0.4217	0.2885	0.2318
AGC [67]	0.3174	0.2136	0.1356	0.1846	0.1099	0.0704	0.5272	0.4836	0.3748	0.5782	0.3467	0.2956
BDF [39]	0.3479	0.2259	0.1674	<u>0.1958</u>	<u>0.1353</u>	<u>0.0896</u>	0.4759	0.4062	0.3014	0.5942	0.3248	0.3113
Ours	<b>0.6817</b>	<b>0.5836</b>	<b>0.5278</b>	<b>0.2664</b>	<b>0.2364</b>	<b>0.1311</b>	<b>0.6573</b>	<b>0.6133</b>	<b>0.5283</b>	<b>0.7962</b>	<b>0.7184</b>	<b>0.6016</b>

Dataset Metric	REUTERS [75]			AudioSet-20 [77]			AudioSet-Music [77]			AudioSet-Human [77]		
	ACC	NMI	ARI	ACC	NMI	ARI	ACC	NMI	ARI	ACC	NMI	ARI
K-means [5]	0.5329	0.3275	0.2593	0.2074	0.1901	0.0780	0.2231	0.1967	0.0742	0.2375	0.2023	0.0840
SpecC [10]	0.4357	0.2948	0.2214	0.2195	0.1774	0.0741	0.2264	0.1897	0.0823	0.2254	0.1836	0.0752
DBSCAN [12]	0.4197	0.2564	0.2164	0.1300	0.1033	0.0400	0.1475	0.1054	0.0446	0.1163	0.1024	0.0354
FLM [9]	0.4563	0.2832	0.2635	0.1761	0.1480	0.1002	0.2185	0.1680	0.1097	0.1546	0.1608	0.1049
AGC [67]	0.5956	0.3386	0.3074	0.2087	0.2037	0.1074	0.2424	0.2017	0.1134	0.2246	0.2096	0.1126
BDF [39]	0.6144	0.3523	0.3286	0.2374	0.2106	0.0976	0.2275	0.2264	0.1096	0.2433	0.2227	0.1235
Ours	<b>0.8200</b>	<b>0.7147</b>	<b>0.6154</b>	<b>0.2994</b>	<b>0.2899</b>	<b>0.1685</b>	<b>0.3374</b>	<b>0.3128</b>	<b>0.1812</b>	<b>0.3344</b>	<b>0.2994</b>	<b>0.1818</b>

datasets with higher levels of noise. Fig. 6 illustrates the degradation performance of our method compared to other methods as the noise variance increases. It is clear that our method exhibits a significantly slower degradation rate compared to the other methods.

#### 4.3.2 Performance on Real Datasets

In Tab. 4, we present the quantitative results of our method and the baseline algorithms on the twelve real datasets. Through the analysis of the data in Tab. 4, the following conclusions can be drawn. • Conventional clustering algorithms, including partition-based K-means [5], graph-based SpecC [10], and density-based DBSCAN [12], exhibit inferior clustering performance. • The traditional density-based DBSCAN [12] performs worse than traditional partition-based K-means [5] and graph-based SpecC [10], indicating that there is considerable room for improvement in the traditional DBSCAN algorithm. • Although the latest density-based clustering algorithms, such as FLM [9], have shown significant improvements compared to DBSCAN, they still perform worse than other recently developed graph-based method (AGC [67]), and block-diagonal guided methods (BDF [39]). • Although BDF, and AGC are all recently developed clustering algorithms, AGC exhibit superior clustering performance compared to BDF. This is attributed to the utilization of block-diagonal property in the clustering procedure by AGC. Therefore, researching the block-diagonal property of the similarity graph is meaningful. • Our method outperforms the other methods by a significant margin on all three evaluation metrics for each dataset. The ACC improvement of our method compared to the second best baseline are 2.03%, 19.85%, 5.48%, 19.05%, 28.30%, 7.06%, 6.90%, 17.01%, 12.69%, 5.21%, 8.81% and

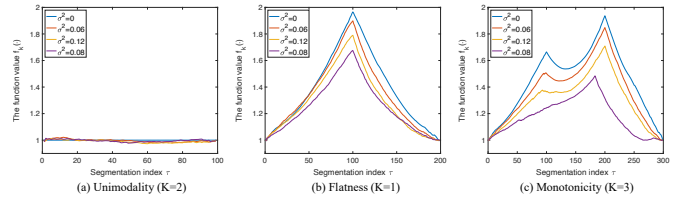


Fig. 7. The function value  $f_k(\tau_k; \tau_k)$  v.s. the segmentation  $\tau_k$ . Verify (a) Unimodality in Proposition 1; (b) Flatness in Proposition 2; (c) Monotonicity in Proposition 3.

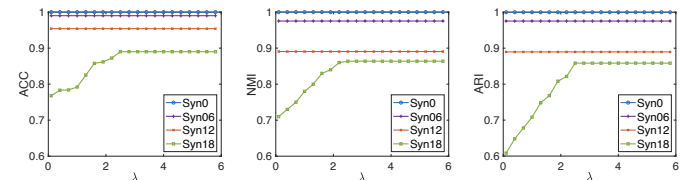


Fig. 8. Clustering performance v.s. the trade-off parameter  $\lambda$ .

8.91% respectively. The NMI improvement of our method compared to the second best baseline are 2.61%, 18.73%, 8.08%, 19.39%, 33.09%, 10.11%, 8.07%, 31.30%, 31.05%, 6.54%, 6.75%, %, % and 6.10% respectively. The ARI improvement of our method compared to the second best baseline are 3.63%, 15.32%, 13.47%, 10.82%, 30.41%, 4.15%, 5.04%, 23.32%, 23.28%, 5.17%, 4.64%, %, % and 5.36% respectively. • Our method demonstrates dramatic superiorities on the ImageNet and AudioSet datasets, implying its suitability for large-scale datasets, not limited to simple datasets like MNIST or COIL20. • Our method achieves competitive results on image, text, and audio datasets simultaneously, highlighting its effectiveness in handling general clustering tasks in practical applications.

TABLE 5  
The ablation experiments of our BD-DBSCAN on three stages.

Dataset	MNIST [69]			CIFAR-10 [70]			COIL-20 [71]			STL-10 [72]		
	Metric	ACC	NMI	ARI	ACC	NMI	ARI	ACC	NMI	ARI	ACC	NMI
1 Ours(I)+AGC [67]	0.8356	0.7428	0.7059	0.3451	0.2436	0.1738	0.8549	0.8373	0.7643	0.3014	0.2954	0.1438
2 BDF+Ours(II,III)	0.9431	0.9129	0.9239	0.2783	0.2139	0.1417	0.9516	0.8822	0.8476	0.2954	0.2114	0.2952
3 Ours(I,II)+ES	0.9852	0.9611	0.9534	0.4828	0.4419	0.3399	0.9962	0.9854	0.9703	0.4819	0.4043	0.2894
4 Ours(I,II,III)	0.9852	0.9611	0.9534	0.4828	0.4419	0.3399	0.9962	0.9854	0.9703	0.4819	0.4043	0.2894

Variance	ImageNet-10 [73]			ImageNet-Dog [73]			20NEWS [74]			REUTERS-10k [75]		
	Metric	ACC	NMI	ARI	ACC	NMI	ARI	ACC	NMI	ARI	ACC	NMI
1 Ours(I)+AGC	0.3871	0.2959	0.2634	0.1818	0.1313	0.1016	0.4719	0.4163	0.3111	0.5812	0.4218	0.3613
2 BDF+Ours(II,III)	0.3947	0.3517	0.3217	0.1415	0.1433	0.0862	0.5499	0.4674	0.4526	0.6054	0.4353	0.4425
3 Ours(I,II)+ES	0.6817	0.5836	0.5278	0.2664	0.2364	0.1311	0.6573	0.6133	0.5283	0.7962	0.7184	0.6016
4 Ours(I,II,III)	0.6817	0.5836	0.5278	0.2664	0.2364	0.1311	0.6573	0.6133	0.5283	0.7962	0.7184	0.6016

Variance	REUTERS [75]			AudioSet-20 [77]			AudioSet-Music [77]			AudioSet-Human [77]		
	Metric	ACC	NMI	ARI	ACC	NMI	ARI	ACC	NMI	ARI	ACC	NMI
1 Ours(I)+AGC	0.6034	0.3963	0.3416	0.2073	0.1906	0.0996	0.2775	0.2664	0.1097	0.2403	0.2327	0.1031
2 BDF+Ours(II,III)	0.5811	0.3846	0.3934	0.2471	0.2115	0.1218	0.2416	0.2353	0.1448	0.2373	0.2431	0.1296
3 Ours(I,II)+ES	0.8200	0.7147	0.6154	0.2994	0.2899	0.1685	0.3374	0.3128	0.1812	0.3344	0.2994	0.1818
4 Ours(I,II,III)	0.8200	0.7147	0.6154	0.2994	0.2899	0.1685	0.3374	0.3128	0.1812	0.3344	0.2994	0.1818

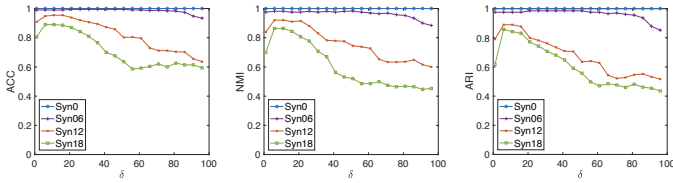


Fig. 9. Clustering performance v.s. minimum number of points in the neighborhood  $\delta$ .

#### 4.3.3 Theoretical Verification

This paper selects synthetic datasets with noise variances (0, 0.06, 0.12, 0.18) to verify the proposed theory and propositions. Theorem 1 indicates that the graph generated by our method will exhibit a block-diagonal form after a specific permutation. This is demonstrated in Fig. 5. However, we have observed that as the level of noise in the data increases, the block-diagonal form becomes less evident. This is because our graph construction algorithm does not impose a constraint on the number of diagonal blocks during the graph construction process. As a result, when constructing the graph, the algorithm may mistakenly perceive fewer diagonal blocks (less than  $K$ ) due to the interference caused by noise. Consequently, the generated graph still presents a block-diagonal form, but with blurred diagonal blocks.

We have selected  $K = 1, 2, 3$  clusters from the synthetic datasets and illustrate the variation of  $f_k(\tau_k; \tau_{-k})$  with respect to  $\tau_k$ . Fig. 7 illustrates the relationship between the function value  $f_k(\tau_k; \tau_{-k})$  and the segmentation  $\tau_k$ . As shown in Fig. 7, when the noise level is relatively low, the curve is nearly flat, unimodal, and monotonic. However, as the noise increases, the curve exhibits some degree of fluctuation.

#### 4.4 Parameter Sensitivity Analysis

This paper selects synthetic datasets with noise variances (0, 0.06, 0.12, 0.18) to study the sensitivity of our method to its parameters.

##### 4.4.1 Effect and Estimation of $\lambda$

We fix  $\delta = 10$  and plot the relationship between  $\lambda$  and the three clustering metrics. As shown in Fig. 8, the clustering performance remains unchanged for datasets with

lower noise levels as  $\lambda$  increases. However, for the synthetic dataset with a noise variance of 0.18, the clustering performance improves as  $\lambda$  increases. Therefore, we conclude that the weighting parameter  $\lambda$  should be set to a small value for clean data, and relatively larger values for data contaminated with heavy noise.

##### 4.4.2 Effect and Estimation of $\delta$

Fig. 9 illustrates the relationship between  $\delta$  and the three clustering metrics. Generally, we observe that setting  $\delta \in \{10, 11, \dots, 30\}$  leads to better clustering results. Additionally, the clustering performance exhibits relatively stable variations when  $\delta$  changes within a small range, indicating that our algorithm is not highly sensitive to the parameter  $\delta$ . Furthermore, we observe that datasets with lower noise levels exhibit a higher tolerance to variations in the  $\delta$  parameter. In other words,  $\delta$  can vary within a relatively larger range without significantly affecting the clustering results on the dataset with a low noise level.

#### 4.5 Ablation Study

Our method consists of three stages. Tab. 5 presents the ablation study of our method on these three stages. We draw the following conclusions. • Comparing Line 1 and Line 4, we observe that integrating our Stage II with Stage III leads to better performance than the graph-based clustering method in AGC [67]. This demonstrates the effectiveness of Stage II and III in our algorithm. • Comparing Line 2 and Line 4, we find that using our Stage I results in better performance than the recently developed block-diagonal guided graph construction method in BDF [39]. Traditional graph construction methods with block-diagonal constraints can be applied to our BD-DBSCAN by replacing our graph construction stage. However, compared to conventional strategies, e.g., BDF [39], our graph construction approach is both efficient and effective. The result has shown that our proposed graph construction method, combined with our graph permutation and segmentation, achieves the best clustering performance. • Comparing Line 3 and Line 4, we discover that using exhaustive search (ES) to find the optimal segmentation of diagonal blocks yields clustering



results consistent with the algorithm in our proposed Stage III. This demonstrates the effectiveness of Stage III in our algorithm. It also validates the optimality of our Alg. 1.

## 5 CONCLUSION

In this paper, we introduce a density-based clustering method called BD-DBSCAN. Our approach involves constructing a similarity graph of the data points that has the potential to exhibit a *block-diagonal* form after a certain permutation. We then propose a cluster traversal algorithm to identify a permutation that rearranges the graph into a *block-diagonal* form. Finally, we present a split-and-refine algorithm to identify the diagonal blocks in the permuted graph. The clustering results are determined based on the identification of these diagonal blocks. The proposed BD-DBSCAN clustering method offers a comprehensive set of advantages, consistently achieving the highest clustering performance across various synthetic and real-world benchmark datasets.

## REFERENCES

- [1] A. K. Jain, M. N. Murty, and P. J. Flynn, "Data clustering: a review," *ACM computing surveys (CSUR)*, vol. 31, no. 3, pp. 264–323, 1999.
- [2] D. Xu and Y. Tian, "A comprehensive survey of clustering algorithms," *Annals of Data Science*, vol. 2, no. 2, pp. 165–193, 2015.
- [3] Z. Xing and W. Zhao, "Unsupervised action segmentation via fast learning of semantically consistent actoms," in *Proceedings of the AAAI Conference on Artificial Intelligence*, vol. 38, no. 6, 2024, pp. 6270–6278.
- [4] C. Fraley and A. E. Raftery, "How many clusters? which clustering method? answers via model-based cluster analysis," *The computer journal*, vol. 41, no. 8, pp. 578–588, 1998.
- [5] J. MacQueen, "Classification and analysis of multivariate observations," in *5th Berkeley Symp. Math. Statist. Probability*, 1967, pp. 281–297.
- [6] V. Menon, G. Muthukrishnan, and S. Kalyani, "Subspace clustering without knowing the number of clusters: A parameter free approach," *IEEE Trans. Signal Process.*, vol. 68, pp. 5047–5062, 2020.
- [7] Y. Zhang, S. Ding, L. Wang, Y. Wang, and L. Ding, "Chameleon algorithm based on mutual k-nearest neighbors," *Applied Intelligence*, vol. 51, no. 4, pp. 2031–2044, 2021.
- [8] W. Sun and Q. Du, "Graph-regularized fast and robust principal component analysis for hyperspectral band selection," *IEEE Transactions on Geoscience and Remote Sensing*, vol. 56, no. 6, pp. 3185–3195, 2018.
- [9] T. Qiu and Y.-J. Li, "Fast ldp-mst: An efficient density-peak-based clustering method for large-size datasets," *IEEE Trans. Knowl. Data Eng.*, vol. 35, no. 5, pp. 4767–4780, 2022.
- [10] U. Von Luxburg, "A tutorial on spectral clustering," *Statistics and computing*, vol. 17, no. 4, pp. 395–416, 2007.
- [11] L. Bai, J. Liang, and Y. Zhao, "Self-constrained spectral clustering," *IEEE Trans. Pattern Anal. Mach. Intell.*, 2022.
- [12] M. Ester, H.-P. Kriegel, J. Sander, X. Xu *et al.*, "A density-based algorithm for discovering clusters in large spatial databases with noise." in *kdd*, vol. 96, no. 34, 1996, pp. 226–231.
- [13] R. J. Campello, D. Moulavi, and J. Sander, "Density-based clustering based on hierarchical density estimates," in *Pacific-Asia conference on knowledge discovery and data mining*, 2013, pp. 160–172.
- [14] D. Birant and A. Kut, "St-dbscan: An algorithm for clustering spatial-temporal data," *Data & knowledge engineering*, vol. 60, no. 1, pp. 208–221, 2007.
- [15] A. S. Georghiades, P. N. Belhumeur, and D. J. Kriegman, "From few to many: Illumination cone models for face recognition under variable lighting and pose," *IEEE Trans. Pattern Anal. Mach. Intell.*, vol. 23, no. 6, pp. 643–660, 2001.
- [16] T. Zhou, H. Fu, C. Gong, L. Shao, F. Porikli, H. Ling, and J. Shen, "Consistency and diversity induced human motion segmentation," *IEEE Trans. Pattern Anal. Mach. Intell.*, vol. 45, no. 1, pp. 197–210, 2022.
- [17] Y. Qin, X. Zhang, L. Shen, and G. Feng, "Maximum block energy guided robust subspace clustering," *IEEE Trans. Pattern Anal. Mach. Intell.*, vol. 45, no. 2, 2022.
- [18] Y. Bai, L. Wang, Y. Liu, Y. Yin, H. Di, and Y. Fu, "Human motion segmentation via velocity-sensitive dual-side auto-encoder," *IEEE Trans. Image Process.*, vol. 32, pp. 524 – 536, 2022.
- [19] X. Wang, D. Guo, and P. Cheng, "Support structure representation learning for sequential data clustering," *Pattern Recognition*, vol. 122, p. 108326, 2022.
- [20] M. A. Patwary, D. Palsetia, A. Agrawal, W.-k. Liao, F. Manne, and A. Choudhary, "Scalable parallel optics data clustering using graph algorithmic techniques," in *Proceedings of the International Conference on High Performance Computing, Networking, Storage and Analysis*, 2013, pp. 1–12.
- [21] X. Yang, C. Deng, F. Zheng, J. Yan, and W. Liu, "Deep spectral clustering using dual autoencoder network," in *Proceedings of the IEEE/CVF conference on computer vision and pattern recognition*, 2019, pp. 4066–4075.
- [22] H. Jiang, "Density level set estimation on manifolds with DBSCAN," in *International Conference on Machine Learning*, 2017, pp. 1684–1693.
- [23] H. Jiang and J. Jang, "Faster dbscan via subsampled similarity queries," 2020.
- [24] M. M. A. Patwary, D. Palsetia, A. Agrawal, W.-k. Liao, F. Manne, and A. Choudhary, "A new scalable parallel DBSCAN algorithm using the disjoint-set data structure," in *SC'12: Proceedings of the International Conference on High Performance Computing, Networking, Storage and Analysis*, 2012, pp. 1–11.
- [25] M. M. A. Patwary, N. Satish, N. Sundaram, F. Manne, S. Habib, and P. Dubey, "Pardicle: Parallel approximate density-based clustering," in *Proceedings of the International Conference for High Performance Computing, Networking, Storage and Analysis*, ser. SC '14. Piscataway, NJ, USA: IEEE Press, 2014, pp. 560–571. [Online]. Available: <http://dx.doi.org/10.1109/SC.2014.51>
- [26] M. Muja and D. G. Lowe, "Scalable nearest neighbor algorithms for high dimensional data," *IEEE Trans. Pattern Anal. Mach. Intell.*, vol. 36, no. 11, pp. 2227–2240, 2014.
- [27] A. Sarma, P. Goyal, S. Kumari, A. Wani, J. S. Challa, S. Islam, and N. Goyal, " $\mu$ DBSCAN: An exact scalable DBSCAN algorithm for big data exploiting spatial locality," in *2019 IEEE International Conference on Cluster Computing (CLUSTER)*. IEEE, 2019, pp. 1–11.
- [28] A. Sharma and A. Sharma, "KNN-DBSCAN: Using k-nearest neighbor information for parameter-free density based clustering," in *2017 International Conference on Intelligent Computing, Instrumentation and Control Technologies (ICICT)*, 2017, pp. 787–792.
- [29] M. M. A. Patwary, S. Byna, N. R. Satish, N. Sundaram, Z. Lukić, V. Roytershteyn, M. J. Anderson, Y. Yao, Prabhat, and P. Dubey, "BD-CATS: Big data clustering at trillion particle scale," in *Proceedings of the International Conference for High Performance Computing, Networking, Storage and Analysis*, ser. SC' 15. New York, NY, USA: ACM, 2015, pp. 6:1–6:12. [Online]. Available: <http://doi.acm.org/10.1145/2807591.2807616>
- [30] B. Welton, E. Samanas, and B. P. Miller, "Extreme scale density-based clustering using a tree-based network of gpgpu nodes," in *SC'13: Proceedings of the International Conference on High Performance Computing, Networking, Storage and Analysis*, 2013, pp. 1–11.
- [31] J. Feng, Z. Lin, H. Xu, and S. Yan, "Robust subspace segmentation with block-diagonal prior," in *Proceedings of the IEEE conference on computer vision and pattern recognition*, 2014, pp. 3818–3825.
- [32] F. Wu, Y. Hu, J. Gao, Y. Sun, and B. Yin, "Ordered subspace clustering with block-diagonal priors," *IEEE Trans. Cybern.*, vol. 46, no. 12, pp. 3209–3219, 2015.
- [33] M. Lee, J. Lee, H. Lee, and N. Kwak, "Membership representation for detecting block-diagonal structure in low-rank or sparse subspace clustering," in *Proceedings of the IEEE conference on computer vision and pattern recognition*, 2015, pp. 1648–1656.
- [34] X. Xie, X. Guo, G. Liu, and J. Wang, "Implicit block diagonal low-rank representation," *IEEE Trans. Image Process.*, vol. 27, no. 1, pp. 477–489, 2017.
- [35] C. Lu, J. Feng, Z. Lin, T. Mei, and S. Yan, "Subspace clustering by block diagonal representation," *IEEE Trans. Pattern Anal. Mach. Intell.*, vol. 41, no. 2, pp. 487–501, 2018.
- [36] C. Yang, Z. Ren, Q. Sun, M. Wu, M. Yin, and Y. Sun, "Joint correntropy metric weighting and block diagonal regularizer for robust multiple kernel subspace clustering," *Information Sciences*, vol. 500, pp. 48–66, 2019.

- [37] M. Liu, Y. Wang, J. Sun, and Z. Ji, "Structured block diagonal representation for subspace clustering," *Applied Intelligence*, vol. 50, pp. 2523–2536, 2020.
- [38] L. Wang, J. Huang, M. Yin, R. Cai, and Z. Hao, "Block diagonal representation learning for robust subspace clustering," *Information Sciences*, vol. 526, pp. 54–67, 2020.
- [39] Y. Qin, G. Feng, Y. Ren, and X. Zhang, "Block-diagonal guided symmetric nonnegative matrix factorization," *IEEE Trans. Knowl. Data Eng.*, 2021.
- [40] Y. Lin and S. Chen, "Convex subspace clustering by adaptive block diagonal representation," *IEEE Trans. Neural Netw. Learn. Syst.*, 2022.
- [41] M. Liu, Y. Wang, J. Sun, and Z. Ji, "Adaptive low-rank kernel block diagonal representation subspace clustering," *Applied Intelligence*, vol. 52, no. 2, pp. 2301–2316, 2022.
- [42] Y. Qin, H. Wu, J. Zhao, and G. Feng, "Enforced block diagonal subspace clustering with closed form solution," *Pattern Recognition*, vol. 130, p. 108791, 2022.
- [43] W. Sun, J. Peng, G. Yang, and Q. Du, "Correntropy-based sparse spectral clustering for hyperspectral band selection," *IEEE Geoscience and Remote Sensing Letters*, vol. 17, no. 3, pp. 484–488, 2019.
- [44] Y. Xu, S. Chen, J. Li, C. Xu, and J. Yang, "Fast subspace clustering by learning projective block diagonal representation," *Pattern Recognition*, vol. 135, p. 109152, 2023.
- [45] X. Li, Y. Sun, Q. Sun, and Z. Ren, "Enforced block diagonal graph learning for multikernel clustering," *IEEE Trans. Comput. Soc. Syst.*, 2023.
- [46] Z. Kong, D. Chang, Z. Fu, J. Wang, Y. Wang, and Y. Zhao, "Projection-preserving block-diagonal low-rank representation for subspace clustering," *Neurocomputing*, vol. 526, pp. 19–29, 2023.
- [47] S. Li, Z. Liu, L. Fang, and Q. Li, "Block diagonal representation learning for hyperspectral band selection," *IEEE Trans. Geosci. Remote Sens.*, 2023.
- [48] M. Yin, W. Liu, M. Li, T. Jin, and R. Ji, "Cauchy loss induced block diagonal representation for robust multi-view subspace clustering," *Neurocomputing*, vol. 427, pp. 84–95, 2021.
- [49] M. Liu, Y. Wang, V. Palade, and Z. Ji, "Multi-view subspace clustering network with block diagonal and diverse representation," *Information Sciences*, vol. 626, pp. 149–165, 2023.
- [50] Z. Xie and L. Wang, "Active block diagonal subspace clustering," *IEEE Access*, vol. 9, pp. 83 976–83 992, 2021.
- [51] A. Taştan, M. Muma, and A. M. Zoubir, "Fast and robust sparsity-aware block diagonal representation," *IEEE Trans. Signal Process.*, 2023.
- [52] X. Zhang, X. Xue, H. Sun, Z. Liu, L. Guo, and X. Guo, "Robust multiple kernel subspace clustering with block diagonal representation and low-rank consensus kernel," *Knowledge-Based Systems*, vol. 227, p. 107243, 2021.
- [53] L. Fan, G. Lu, T. Liu, and Y. Wang, "Block diagonal least squares regression for subspace clustering," *Electronics*, vol. 11, no. 15, p. 2375, 2022.
- [54] Y. Xu, S. Chen, J. Li, Z. Han, and J. Yang, "Autoencoder-based latent block-diagonal representation for subspace clustering," *IEEE Trans. Cybern.*, vol. 52, no. 6, pp. 5408–5418, 2020.
- [55] J. Liu, Y. Sun, and Y. Hu, "Deep subspace clustering with block diagonal constraint," *Applied Sciences*, vol. 10, no. 24, p. 8942, 2020.
- [56] J. Liu, X. Liu, Y. Zhang, P. Zhang, W. Tu, S. Wang, S. Zhou, W. Liang, S. Wang, and Y. Yang, "Self-representation subspace clustering for incomplete multi-view data," in *Proceedings of the 29th ACM International Conference on Multimedia*, 2021, pp. 2726–2734.
- [57] J. Zhang, C.-G. Li, T. Du, H. Zhang, and J. Guo, "Convolutional subspace clustering network with block diagonal prior," *IEEE Access*, vol. 8, pp. 5723–5732, 2019.
- [58] S. Li and H. Mehrabadi, "Generation of block diagonal forms using hierarchical clustering for cell formation problems," *Procedia CIRP*, vol. 17, pp. 44–49, 2014.
- [59] R. Fu and Z. Li, "An evidence accumulation based block diagonal cluster model for intent recognition from eeg," *Biomedical Signal Processing and Control*, vol. 77, p. 103835, 2022.
- [60] C. Chen and S. Irani, "Cluster first-sequence last heuristics for generating block diagonal forms for a machine-part matrix," *THE INTERNATIONAL JOURNAL OF PRODUCTION RESEARCH*, vol. 31, no. 11, pp. 2623–2647, 1993.
- [61] J. Chen and J. G. Dy, "A generative block-diagonal model for clustering," in *UAI*, 2016.
- [62] C. Chen, J. Wei, and Z. Li, "Multiple kernel k-means clustering with block diagonal property," *Pattern Analysis and Applications*, vol. 26, no. 3, pp. 1515–1526, 2023.
- [63] S.-S. Choi, S.-H. Cha, and C. C. Tappert, "A survey of binary similarity and distance measures," *Journal of systemics, cybernetics and informatics*, vol. 8, no. 1, pp. 43–48, 2010.
- [64] W. Sun, J. Peng, G. Yang, and Q. Du, "Fast and latent low-rank subspace clustering for hyperspectral band selection," *IEEE Transactions on Geoscience and Remote Sensing*, vol. 58, no. 6, pp. 3906–3915, 2020.
- [65] E. G. Birgin, J. M. Martínez, and M. Raydan, "Nonmonotone spectral projected gradient methods on convex sets," *SIAM Journal on Optimization*, vol. 10, no. 4, pp. 1196–1211, 2000.
- [66] J. Shi and J. Malik, "Normalized cuts and image segmentation," *IEEE Trans. Pattern Anal. Mach. Intell.*, vol. 22, no. 8, pp. 888–905, 2000.
- [67] N. Mrabah, M. Bouguessa, M. F. Touati, and R. Ksantini, "Rethinking graph auto-encoder models for attributed graph clustering," *IEEE Trans. Knowl. Data Eng.*, vol. 35, no. 5, pp. 5076–5090, 2022.
- [68] S. Tierney, J. Gao, and Y. Guo, "Subspace clustering for sequential data," in *Proceedings of the IEEE conference on computer vision and pattern recognition*, 2014, pp. 1019–1026.
- [69] Y. LeCun, L. Bottou, Y. Bengio, and P. Haffner, "Gradient-based learning applied to document recognition," *Proceedings of the IEEE*, vol. 86, no. 11, pp. 2278–2324, 1998.
- [70] A. Krizhevsky, G. Hinton *et al.*, "Learning multiple layers of features from tiny images," 2009.
- [71] S. A. Nene, S. K. Nayar, H. Murase *et al.*, "Columbia object image library (coil-100)," 1996.
- [72] A. Coates, A. Ng, and H. Lee, "An analysis of single-layer networks in unsupervised feature learning," in *Proceedings of the fourteenth international conference on artificial intelligence and statistics*, 2011, pp. 215–223.
- [73] J. Deng, W. Dong, R. Socher, L.-J. Li, K. Li, and L. Fei-Fei, "Imagenet: A large-scale hierarchical image database," in *2009 IEEE conference on computer vision and pattern recognition*, 2009, pp. 248–255.
- [74] K. Lang, "Newsweeder: Learning to filter netnews," in *Machine learning proceedings 1995*, 1995, pp. 331–339.
- [75] D. D. Lewis, Y. Yang, T. Russell-Rose, and F. Li, "Rcv1: A new benchmark collection for text categorization research," *Journal of machine learning research*, vol. 5, no. Apr, pp. 361–397, 2004.
- [76] J. Xie, R. Girshick, and A. Farhadi, "Unsupervised deep embedding for clustering analysis," in *International conference on machine learning*, 2016, pp. 478–487.
- [77] J. F. Gemmeke, D. P. Ellis, D. Freedman, A. Jansen, W. Lawrence, R. C. Moore, M. Plakal, and M. Ritter, "Audio set: An ontology and human-labeled dataset for audio events," in *2017 IEEE international conference on acoustics, speech and signal processing (ICASSP)*, 2017, pp. 776–780.



GLOBALCOM, WCNC, ICASSP, AAAI, and TSP.

**Zheng Xing** received the B.Eng. degree from Ocean University of China, Qingdao, China, in 2017, and the M.Eng. degree from Beihang University, Beijing, China, in 2020. He is currently pursuing the Ph.D. degree at The Chinese University of Hong Kong, Shenzhen, China. His research interests focus on data analysis, subspace clustering, indoor localization, trajectory recovery, and human motion segmentation, in the field of which he has published multiple papers in top conferences or journals, such as



nals, including ICCV, ECCV, AAAI, IJCAI, MM, and TNNLS.

**Weibing Zhao** received the B.S. degree in computer science and technology from the School of Information Science and Technology, Beijing Normal University, Beijing, China, in 2018. She obtained his Ph.D. degree from The Chinese University of Hong Kong, Shenzhen, China, in 2024. Currently, she holds the position of Associate Professor at Shenzhen MSU-BIT University. Her research interests encompass data analysis and 3-D computer vision, and she has contributed to multiple top conferences or journals,

## APPENDIX

### .1 Proof of Theorem 1

Let  $\tilde{\mathbf{Z}} = \mathbf{\Gamma}^{-1}\mathbf{Z}\mathbf{\Gamma}$ . From the properties of permutation matrices, we have  $\mathbf{\Gamma}^{-1} = \mathbf{\Gamma}^T$  and  $\mathbf{\Gamma}\mathbf{e} = \mathbf{e}$ , thus  $f(\mathbf{Z}) = \|\mathbf{X}\mathbf{Z} - \mathbf{X}\|_{\mathbb{F}}^2 + \lambda_1 \mathbf{e}^T \mathbf{Z}^T \mathbf{Z} \mathbf{e} = \|\tilde{\mathbf{X}}\tilde{\mathbf{Z}} - \tilde{\mathbf{X}}\|_{\mathbb{F}}^2 + \lambda_1 \mathbf{e}^T \tilde{\mathbf{Z}}^T \tilde{\mathbf{Z}} \mathbf{e}$ . Hence if we take  $\tilde{\mathbf{X}}$  as the data matrix instead of  $\mathbf{X}$ , then the solution to Problem (1) is  $\tilde{\mathbf{Z}}^*$ . Therefore we assume, without loss of generality, the columns of  $\mathbf{X}$  are in general position:  $\mathbf{X} = [\mathbf{X}_1, \mathbf{X}_2, \dots, \mathbf{X}_K]$ , where all the columns of sub-matrix  $\mathbf{X}_\alpha$  lie in the same subspace  $\mathcal{S}_\alpha$ .

Assume  $\mathbf{Z}^*$  is the optimal solution, and we decompose  $\mathbf{Z}^*$  to be the sum of two matrices

$$\mathbf{Z}^* = \mathbf{Z}^D + \mathbf{Z}^C$$

$$= \begin{bmatrix} \mathbf{Z}_{11}^* & & & \mathbf{0} \\ & \mathbf{Z}_{22}^* & & \\ & & \ddots & \\ \mathbf{0} & & & \mathbf{Z}_{KK}^* \end{bmatrix} + \begin{bmatrix} \mathbf{0} & \mathbf{Z}_{12}^* & \cdots & \mathbf{Z}_{1K}^* \\ \mathbf{Z}_{21}^* & \mathbf{0} & \cdots & \mathbf{Z}_{2K}^* \\ \vdots & \vdots & \ddots & \vdots \\ \mathbf{Z}_{K1}^* & \mathbf{Z}_{K2}^* & \cdots & \mathbf{0} \end{bmatrix}$$

where  $\mathbf{Z}_{ij}^* \in \mathbb{R}^{\mathcal{N}_i \times \mathcal{N}_j}$ . Note that both  $\mathbf{Z}^D$  and  $\mathbf{Z}^C$  are non-negative.

According to the decomposition of  $\mathbf{Z}^*$ , any column of  $\mathbf{Z}^*$  can be written as  $\mathbf{z}_i^* = \mathbf{z}_i^D + \mathbf{z}_i^C$ , with  $\mathbf{z}_i^D$  and  $\mathbf{z}_i^C$  supported on disjoint subset of indexes. We can write  $\|\mathbf{X}\mathbf{Z}^* - \mathbf{X}\|_{\mathbb{F}}^2$  as  $\sum_{i=1}^N \|\mathbf{X}\mathbf{z}_i^D - \mathbf{x}_i\|_2^2 + \sum_{i=1}^N \|\mathbf{X}\mathbf{z}_i^C\|_2^2 + 2 \sum_{i=1}^N \cos\theta_i \|\mathbf{X}\mathbf{z}_i^D - \mathbf{x}_i\|_2 \|\mathbf{X}\mathbf{z}_i^C\|_2$ , where  $\theta_i$  is the angle between vector  $\mathbf{X}\mathbf{z}_i^D - \mathbf{x}_i$  and  $\mathbf{X}\mathbf{z}_i^C$ .

Since the matrix  $\mathbf{X} = [\mathbf{X}_1, \mathbf{X}_2, \dots, \mathbf{X}_K]$  is well arranged, any column  $\mathbf{x}_i \in \mathbf{X}_\alpha$  and  $\mathbf{x}_j \in \mathbf{X}_\beta$  lie in different subspaces if  $\alpha \neq \beta$ . Let  $\mathbf{x}_i \in \mathcal{S}_\alpha$ , according to the definition of  $\mathbf{z}_i^D$  and  $\mathbf{z}_i^C$ , we have  $\mathbf{X}\mathbf{z}_i^D \in \mathcal{S}_\alpha$  and  $\mathbf{X}\mathbf{z}_i^C \notin \mathcal{S}_\alpha$ . Based on the orthogonal subspace assumption, we have  $(\mathbf{X}\mathbf{z}_i^D - \mathbf{x}_i) \perp \mathbf{X}\mathbf{z}_i^C$  and  $\theta_i = \pi/2$ , thus  $\|\mathbf{X}\mathbf{Z}^* - \mathbf{X}\|_{\mathbb{F}}^2 = \|\mathbf{X}\mathbf{Z}^D - \mathbf{X}\|_{\mathbb{F}}^2 + \|\mathbf{X}\mathbf{Z}^C\|_{\mathbb{F}}^2 \geq \|\mathbf{X}\mathbf{Z}^D - \mathbf{X}\|_{\mathbb{F}}^2$ .

Based on the non-negativity of  $\mathbf{Z}^*$ ,  $\mathbf{Z}^C$ , and  $\mathbf{Z}^D$ , we have  $\|(\mathbf{Z}^*)^T \mathbf{Z}^* \mathbf{1}\|_1 = \sum_{i,j} |(\mathbf{z}_i^*)^T \mathbf{z}_j^*| \geq \|(\mathbf{z}^D)^T \mathbf{z}^D \mathbf{1}\|_1$ .

From the above two inequalities, we have  $f(\mathbf{Z}^*) \geq f(\mathbf{Z}^D)$ . Because  $\mathbf{Z}^*$  is the optimal, we have  $f(\mathbf{Z}^*) = f(\mathbf{Z}^D)$  and  $\mathbf{Z}^C = \mathbf{0}$ , thus  $\mathbf{Z}^* = \mathbf{Z}^D$ . Hence the optimal solution to Problem (1) is block-diagonal and Theorem 1 holds.

### .2 Proof of Proposition 1

Without loss of generality, suppose  $k = 1$ , and  $\tau_{k-1} = t_0, \tau_{k+1} = t_2, t_j = t_1$ . Consider  $\tau \in (0, t_1]$ , we have

$$f_1(\tau) = \frac{(t_1 - \tau)^2 \mu_1 + (t_2 - t_1)^2 \mu_2}{(t_1 - \tau)t_1 \mu_1 + (t_2 - t_1)^2 \mu_2} + \frac{t^2 \mu_1}{\tau t_1 \mu_1}$$

$$= \frac{\tau}{t_1} + \frac{1 + (t_1 - \tau)^2 C_1}{1 + (t_1 - \tau)t_1 C_1}$$

where  $C_1 = \frac{\mu_1}{(t_2 - t_1)^2 \mu_2}$ . Then, we have

$$f_1(\tau) = \frac{\tau(1 + (t_1 - \tau)t_1 C_1) + t_1(1 + (t_1 - \tau)^2 C_1)}{t_1(1 + (t_1 - \tau)t_1 C_1)}$$

$$= 1 + \frac{1}{(1 + t_1^2 C_1)t_1 \tau^{-1} - t_1^2 C_1}$$

The function  $f_1(\tau)$  is monotonically increasing for  $\tau \in (0, t_1]$ .

Consider  $\tau \in [t_1, t_2)$ , we have

$$f_1(\tau) = \frac{(t_2 - \tau)^2 \mu_1}{(t_2 - \tau)(t_2 - t_1)\mu_1}$$

$$+ \frac{t_1^2 \mu_1 + (t_2 - t_1)^2 \mu_2 + (\tau - t_1)^2 \mu_2}{t_1^2 \mu_1 + (t_2 - t_1)^2 \mu_2 + (\tau - t_1)(t_2 - t_1)\mu_2}$$

$$= \frac{t_2 - \tau}{t_2 - t_1} + \frac{1 + (\tau - t_1)^2 C_2}{1 + (\tau - t_1)(t_2 - t_1)C_2}$$

where  $C_2 = \frac{\mu_2}{t_1^2 \mu_1 + (t_2 - t_1)^2 \mu_2}$ . Then, we have

$$f_1(\tau) = 1 + \frac{t_2 - \tau}{t_2 - t_1 + (t_2 - t_1)^2 C_2 (\tau - t_1)}$$

$$= 1 + \frac{1}{\Delta_{21}(1 + \Delta_{21}^2 C_2)(t_2 - \tau)^{-1} - \Delta_{21}^2 C_2}$$

where  $\Delta_{21} = t_2 - t_1$ . The function  $f_1(\tau)$  is monotonically decreasing for  $\tau \in [t_1, t_2)$ .

### .3 Proof of Proposition 2

Without loss of generality, suppose  $k = 1$ , and  $\tau_{k-1} = t_0, \tau_{k+1} = t_1$ .

$$f_1(\tau) = \frac{\sum_{i,j \in [1, \tau]} w_{i,j}}{\sum_{i \in [1, \tau]} \sum_{j \in [1, t_1]} w_{i,j}} + \frac{\sum_{i,j \in [\tau+1, t_1]} w_{i,j}}{\sum_{i \in [\tau+1, t_1]} \sum_{j \in [1, t_1]} w_{i,j}}$$

$$= \frac{\tau^2 \mu_1}{\tau t_1 \mu_1} + \frac{(t_1 - \tau)^2 \mu_1}{(t_1 - \tau)t_1 \mu_1} = 1$$

The function  $f_1(\tau)$  is constant for  $\tau \in (t_0, t_1)$ .

### .4 Proof of Proposition 3

Without loss of generality, suppose  $k = 1$ , and  $\tau_{k-1} = 0, \tau_{k+1} = t_L, L \geq 3$ .

• Consider  $\tau \in (0, t_1]$ , we have

$$f_1(\tau) = \frac{(t_1 - \tau)^2 \mu_1 + (t_2 - t_1)^2 \mu_2 + \dots + (t_L - t_{L-1})^2 \mu_L}{(t_1 - \tau)t_1 \mu_1 + (t_2 - t_1)^2 \mu_2 + \dots + (t_L - t_{L-1})^2 \mu_L}$$

$$+ \frac{\tau^2 \mu_1}{\tau t_1 \mu_1}$$

$$= \frac{\tau}{t_1} + \frac{1 + (t_1 - \tau)^2 C_1}{1 + (t_1 - \tau)t_1 C_1}$$

where  $C_1 = \frac{\mu_1}{(t_L - t_1)^2 b(2, L)}$  and  $b(2, L) = \frac{(t_2 - t_1)^2 \mu_2 + \dots + (t_L - t_{L-1})^2 \mu_L}{(t_L - t_1)^2}$ .  $f_1(\tau)$  can also be written as

$$f_1(\tau) = \frac{\tau(1 + (t_1 - \tau)t_1 C_1) + t_1(1 + (t_1 - \tau)^2 C_1)}{t_1(1 + (t_1 - \tau)t_1 C_1)}$$

$$= \frac{\tau + t_1 + (t_1 - \tau)t_1 C_1 (\tau + t_1 - \tau)}{t_1 + (t_1 - \tau)t_1^2 C_1}$$

$$= \frac{\tau + t_1 + (t_1 - \tau)t_1^2 C_1}{t_1 + (t_1 - \tau)t_1^2 C_1}$$

$$= 1 + \frac{1}{(1 + t_1^2 C_1)t_1 \tau^{-1} - t_1^2 C_1}$$

The function  $f_1(\tau)$  is monotonically increasing for  $\tau \in (0, t_1]$ .

- Consider  $\tau \in [t_{L-1}, t_L]$ , we have

$$\begin{aligned} f_1(\tau) &= \frac{(t_L - \tau)^2 \mu_1}{(t_L - \tau)(t_L - t_{L-1})\mu_1} + \phi \\ &= \frac{(t_L - \tau)^2 \mu_1}{(t_L - \tau)(t_L - t_{L-1})\mu_1} + \phi \\ &= \frac{t_L - \tau}{t_L - t_{L-1}} + \frac{1 + (\tau - t_{L-1})^2 C_2}{1 + (\tau - t_{L-1})(t_L - t_{L-1})C_2} \end{aligned}$$

where

$$C_2 = \frac{\mu_L}{t_{L-1}^2 b(1, L-1)},$$

$$\phi = \frac{t_{L-1}^2 b(1, L-1) + (\tau - t_{L-1})^2 \mu_L}{t_{L-1}^2 b(1, L-1) + (\tau - t_{L-1})(t_L - t_{L-1})\mu_L},$$

and

$$b(1, L-1) = \frac{t_1^2 \mu_1 + (t_2 - t_1)^2 \mu_2 + \dots + (t_{L-1} - t_{L-2})^2 \mu_{L-1}}{t_{L-1}^2}.$$

$f_1(\tau)$  can also be written as

$$\begin{aligned} f_1(\tau) &= 1 + \frac{t_L - \tau}{t_L - t_{L-1} + (t_L - t_{L-1})^2 C_2 (\tau - t_{L-1})} \\ &= 1 + \frac{1}{\Delta_L (1 + \Delta_L^2 C_2) (t_L - \tau)^{-1} - \Delta_L^2 C_2} \end{aligned}$$

where  $\Delta_L = t_L - t_{L-1}$ . The function  $f_1(\tau)$  is monotonically decreasing for  $\tau \in [t_{L-1}, t_L]$ .

- Consider  $\tau \in [t_k, t_{k+1}]$ , for any  $k \in \{1, 2, \dots, L-2\}$ .

$$\begin{aligned} f_1(\tau) &= \frac{t_1^2 \mu_1 + \dots + (t_k - t_{k-1})^2 \mu_k + (\tau - t_k)^2 \mu_{k+1}}{t_1^2 \mu_1 + \dots + (t_k - t_{k-1})^2 \mu_k + (t_{k+1} - t_k)(\tau - t_k) \mu_{k+1}} \\ &+ \frac{(t_{l+2} - t_{k+1})^2 \mu_{l+2} + \dots}{(t_{l+2} - t_{k+1})^2 \mu_{l+2} + \dots} \\ &= \frac{t_k^2 b(1, k) + (\tau - t_k)^2 \mu_{k+1}}{t_k^2 b(1, k) + (t_{k+1} - t_k)(\tau - t_k) \mu_{k+1}} \\ &+ \frac{(t_L - t_{k+1})^2 b(k+2, L) + (t_{k+1} - \tau)^2 \mu_{k+1}}{(t_L - t_{k+1})^2 b(k+2, L) + (t_{k+1} - t)(t_{k+1} - t_k) \mu_{k+1}} \end{aligned}$$

where  $b(1, k) = \frac{t_1^2 \mu_1 + \dots + (t_k - t_{k-1})^2 \mu_k}{t_k^2}$  and  $b(k+2, L) = \frac{(t_{k+2} - t_{k+1})^2 \mu_{k+2} + \dots + (t_L - t_{k+1})^2 \mu_L}{(t_L - t_{k+1})^2}$ . Denote  $d = t_{k+1} - t_k$ , and  $x = \tau - \frac{t_{k+1} + t_k}{2}$ . Since  $\tau \in (t_{k+1}, t_k)$ , we have  $x \in (-\frac{d}{2}, \frac{d}{2})$ . Denote  $B_1 = \frac{\mu_{k+1}}{t_k^2 b(1, k)}$ , and  $B_2 = \frac{\mu_{k+1}}{(t_L - t_{k+1})^2 b(k+2, L)}$ . So,  $f_1(\tau)$  can be written as

$$f(x) = \frac{x^2(-d^2 B_1 B_2 + B_1 + B_2) + 2dx(B_1 - B_2) + \varphi_1}{-x^2 d^2 B_1 B_2 + xd(B_1 - B_2) + \varphi_2}$$

where  $\varphi_1 = \frac{3}{4}d^2(B_1 + B_2) + \frac{d^4}{4}B_1 B_2 + 2$ ,  $\varphi_2 = \frac{d^4}{4}B_1 B_2 + \frac{1}{2}d^2(B_1 + B_2) + 1$ .  $f(x)$  is monotonically decreasing for  $x \leq x_0$ , and monotonically increasing for  $x \geq x_0$ , where

$$x_0 = \begin{cases} \frac{(\sqrt{B_1 d^2 + 1} + \sqrt{B_2 d^2 + 1})^2}{2d(B_2 - B_1)} & B_1 \neq B_2 \\ 0 & B_1 = B_2 \end{cases}$$

Recall the definition of  $d$  and  $x$ , the function  $f_1(\tau)$  is monotonically decreasing for  $\tau \leq \hat{\tau}$ , and monotonically increasing for  $\tau \geq \hat{\tau}$ , where

$$\begin{aligned} \hat{\tau} &= \frac{\left( \sqrt{B_1 (t_{k+1} - t_k)^2 + 1} + \sqrt{B_2 (t_{k+1} - t_k)^2 + 1} \right)^2}{2(t_{k+1} - t_k)(B_2 - B_1)} \\ &+ \frac{1}{2}(t_{k+1} + t_k) \end{aligned}$$

for  $B_1 \neq B_2$ , and  $\frac{1}{2}(t_{k+1} + t_k)$  otherwise. Thus, for the interval  $[t_k, t_{k+1}]$ ,  $k = 1, \dots, L-2$ ,  $f_1(\tau)$  increases for  $\tau \in [t_k, \hat{\tau}]$  and decreases for  $\tau \in [\hat{\tau}, t_{k+1}]$  if  $\hat{\tau} \in (t_k, t_{k+1})$ ;  $f_1(\tau)$  increases for  $\tau \in [t_k, t_{k+1}]$  if  $\hat{\tau} \geq t_{k+1}$ ;  $f_1(\tau)$  decreases for  $\tau \in [t_k, t_{k+1}]$  if  $\hat{\tau} \leq t_k$ .

Consider two distinct intervals  $(\tau_{k-1}^{(m,k)}, \tau_{k+1}^{(m,k)})$  and  $(\tau_{k'-1}^{(m,k')}, \tau_{k'+1}^{(m,k')})$  constructed from the  $m$ th iteration of Step 1) in Alg. 1, where  $\tau_{k-1}^{(m,k)}, \tau_{k+1}^{(m,k)}, \tau_{k'-1}^{(m,k')}, \tau_{k'+1}^{(m,k')} \in t_0, t_1, \dots, t_K$ . Suppose that there exists at least one index  $t_j \in \{t_1, t_2, \dots, t_{K-1}\}$  in  $(\tau_{k-1}^{(m,k)}, \tau_{k+1}^{(m,k)})$ , and no such  $t_j$  in  $(\tau_{k'-1}^{(m,k')}, \tau_{k'+1}^{(m,k')})$ . Then,  $\Delta f_*^{(m,k)} > \Delta f_*^{(m,k')}$ .

## 5 Proof of Lemma 1

Since there exists at least one index  $t_j \in \{t_1, t_2, \dots, t_{K-1}\}$  in  $(\tau_{k-1}^{(m,k)}, \tau_{k+1}^{(m,k)})$ , it thus follows from Proposition 3 that  $\Delta f_*^{(m,k)} = f_*^{(m,k)} - f_k(\tau_{k-1}^{(m,k)}; \tau_{-k}^{(m,k)}) > f_k(\tau; \tau_{-k}^{(m,k)}) - f_k(\tau_{k-1}^{(m,k)}; \tau_{-k}^{(m,k)})$ .

Since there exists no such  $t_j$  in  $(\tau_{k'-1}^{(m,k')}, \tau_{k'+1}^{(m,k')})$ , it thus follows from Proposition 2 that  $\Delta f_*^{(m,k')} = f_*^{(m,k')} - f_{k'}(\tau_{k'-1}^{(m,k')}; \tau_{-k'}^{(m,k')}) = f_{k'}(\tau; \tau_{-k'}^{(m,k')}) - f_{k'}(\tau_{k'-1}^{(m,k')}; \tau_{-k'}^{(m,k')})$ . As a result,  $\Delta f_*^{(m,k)} > \Delta f_*^{(m,k')}$ .

## 6 Proof of Theorem 2

For  $m = 1$ , we split the interval  $(t_0, t_K)$  into two sub-intervals. Proposition 1 indicates that one of  $\{t_1, t_2, \dots, t_{K-1}\}$  will be the first optimal split index.

For  $m = 2$ , suppose the first optimal split index is  $t_1$ , and  $\tau^{(2)} = \{t_1\}$ . We then insert the second split index into the intervals  $(t_0, t_1)$  and  $(t_1, t_K)$ . Lemma 1 indicates that the larger  $\Delta f_*^{(2,k)}$  arises from splitting the interval  $(t_1, t_K)$ , which contains at least one of  $\{t_2, t_3, \dots, t_{K-1}\}$ .

For  $m = 3$ , suppose the second optimal split index is  $t_2$ , and  $\tau^{(3)} = \{t_1, t_2\}$ . We then insert the third split index into the intervals  $(t_0, t_1)$ ,  $(t_1, t_2)$ , and  $(t_2, t_K)$ . The larger  $\Delta f_*^{(3,k)}$  arises from splitting the interval that contains at least one of  $\{t_3, t_4, \dots, t_{K-1}\}$ .

We repeat this process until completing iteration  $m = K - 1$ . Then, we have  $\tau^{(K)} = \{t_1, t_2, \dots, t_{K-1}\}$ .

When we continue inserting splitting indexes for  $m = K$ , Proposition 2 indicates that  $\Delta f_*^{(K,k)}$  is constant for any  $k$  because there are no  $\{t_1, t_2, \dots, t_{K-1}\}$  in any interval  $(t_{k-1}, t_k)$ ,  $k \in 1, 2, \dots, K$ . Thus, the function  $g(m)$  remains constant for any  $m \geq K$ . Since  $g(m)$  is monotonically increasing for  $m < K$ ,  $m = K$  is the only inflection point for the function  $g(m)$ . Consequently, our Alg. 1 will output the true cluster number  $K$ .